Received: 27 July 2022 | Revised: 25 January 2023 | Accepted: 28 January 2023

DOI: 10.1111/jmg.12716

ORIGINAL ARTICLE

Journal of METAMORPHIC GEOLOGY WILEY

To be or not to be Alpine: New petrological constraints on the metamorphism of the Chenaillet Ophiolite (Western Alps)

Alberto Corno[1] | **Chiara Groppo**[1] | **Alessandro Borghi**[1] | **Pietro Mosca**[2] | **Marco Gattiglio**[1]

[1]Department of Earth Sciences, University of Torino, Turin, Italy

[2]Geosciences and Earth Resources - National Research Council of Italy, IGG-CNR, Turin, Italy

Correspondence
Alberto Corno, Department of Earth Sciences, University of Torino, Via Valperga Caluso 35, Turin 10125, Italy.
Email: alberto.corno@unito.it

Funding information
This research was funded by research Grants from University of Torino, RicercaLocale "ex 60%" (A.B. and M.G.) and by Ministero dell'Università e della Ricerca Scientifica e Tecnologica (M.I.U.R.) in the framework of the PhD project of A.C.

Handling Editor: Prof. Clare Warren

Abstract

The Chenaillet Ophiolite represents a very well-preserved portion of Ligurian-Piedmont ocean in the Western Alps. It is formed from an oceanic lithospheric succession comprising exhumed mantle, various mafic intrusives (i.e., gabbro sensu *lato*), and a world-renowned sequence of pillow basalts. Apart from scarce breccias closely related to oceanic lithosphere, no sedimentary cover is exposed. Historically, the Chenaillet Ophiolite has been known for its very low temperature–low pressure Alpine metamorphism, ascribed to obduction processes. However, studies aimed at constraining the peak pressure–temperature (P–T) conditions of Alpine metamorphism are virtually lacking, the general focus having been so far on its high temperature metamorphism and geochemical features. In this paper, we investigate two kinds of rocks: gabbro and albitite/alkali syenite, whose petrographic features shed light on the complex metamorphic history of the Chenaillet Ophiolite. Detailed analyses of mineral assemblages, blastesis/deformation relationships, and mineral chemical data allow two metamorphic events to be distinguished: an earlier, high temperature event (already reported in the literature) and a second, later low temperature, high pressure event, recognized here for the first time. The low temperature, high pressure event is strikingly testified by the occurrence of lawsonite relicts in the gabbro and of interstitial omphacite in the albitite. Thermodynamic modelling (i.e., via isochemical phase diagrams) performed on a gabbro sample suggests for this unit a minimum of 9 kbar and 300°C and a maximum of 15 kbar and 450°C. Overlapping these P–T conditions with those inferred for the albitite based on the observed mineral assemblage allows the Alpine peak metamorphism to be constrained to 10–11 kbar and 340–360°C. These P–T conditions suggest a thickness of the overlying nappe stack of about 35–40 km, which is incompatible with obduction or burial processes, and instead consistent with subduction processes related to the Alpine orogeny.

We argue that, opposite to the common belief that the Chenaillet Ophiolite escaped Alpine metamorphism, our new data strongly support the idea that it experienced low temperature-blueschist-facies metamorphism, whose evidence can still be tracked in those (few) rocks that better recorded and preserved it. This finding generates new challenging questions regarding both subduction and exhumation processes in complex orogens such as the Western Alps.

KEYWORDS
Alpine metamorphism, Chenaillet Ophiolite, P–T isochemical phase diagram, tectono-metamorphic evolution, Western Alps

1 | INTRODUCTION

The Chenaillet Ophiolite (CO hereafter) exposed in the Western Alps is a remnant of the Ligurian-Piedmont oceanic domain (i.e., Alpine Tethys ocean), developed in Middle to Late Jurassic between the European and Apulian plates. It crops out as a thin (i.e., less than 1 km) klippe-like unit at the uppermost structural levels of the tectonic pile, above blueschist-facies unit of the Ligurian-Piedmont ocean. It consists of serpentinized peridotites, ophicarbonate rocks, various intrusive bodies (Mg-gabbro, Fe-gabbro, and alkali syenite/albitite), and large quantities of pillow basalts and their related breccias and dolerites, widely studied and investigated by many generations of geologists (e.g., Buffon, 1786; Chalot-Prat, 2005; Delesse, 1848; Lewis & Smewing, 1980; Mevel, 1975; Mevel & Velde, 1976; Michel-Lévy, 1877; Vuagnat, 1946, 1966, 1975; Vuagnat & Pusztaszeri, 1965).

The ophiolite sequence is only overprinted by weak Alpine metamorphism and deformation so that primary contacts and relationships among different lithologies, as well as original magmatic textures, are well preserved (Manatschal et al., 2011). In addition, this ophiolitic sequence preserves syn-magmatic shear zones, exhumation detachment faults developed along the ocean floor, and high-angle faults related to the extrusion of volcanic rocks (Balestro et al., 2019; Manatschal et al., 2011). Therefore, the CO has been largely regarded by the Alpine literature as a key sector to refine genetic models for the Ligurian-Piedmont ocean, often considering geochemistry, isotope geochronology, magma genesis, and evolution of the oceanic crust (Chalot-Pra & Bourlier, 2005; Costa & Caby, 2001; Lafay et al., 2017; Li et al., 2013; Martin, 1984; Nicollet et al., 2022; Tribuzio et al., 2019).

Numerous researchers have investigated the tectono-metamorphic evolution of the Ligurian-Piedmont units of the Western Alps; however, only a few studies focus on the petrologic and metamorphic features of the CO and, in particular, on its Alpine evolution (Arata et al., 1982). Pusztaszeri (1966) first described the occurrence of the prehnite + pumpellyite + albite + epidote + actinolite assemblage, which was interpreted as related to a weak (i.e., low pressure/low temperature [LT]) Alpine metamorphic event. Also, Mével et al. (1978), focusing on the amphibolitized gabbro, attributed the same mineral assemblage to low-grade Alpine metamorphism. Moreover, Arata et al. (1982) related the blastesis also of local aegirine-augite, Mg-riebeckite, lawsonite, stilpnomelane, titanite, and chlorite to this weak Alpine event. On the other hand, Lewis and Smewing (1980) and Bertrand et al. (1982) related this low-grade mineral assemblage to late-stage crystallization of the intrusive bodies. According to these authors, the intrusive rocks of CO were hydrothermally metamorphosed in two stages, at prehnite-pumpellyite and greenschist facies metamorphic conditions, respectively; hence, subseafloor recrystallization predates the Alpine metamorphic event. Since then, few studies aimed at constraining the Alpine metamorphic peak of this ophiolitic body, which was thought to have escaped most of the Alpine tectono-metamorphic history due to obduction processes (Chalot-Prat, 2005; Lemoine, 1980; Mével et al., 1978).

Mével et al. (1978) first reported also evidence of high temperature (HT) metamorphism in the CO. This metamorphic event has been variably interpreted by different authors. Mével et al. (1978) tentatively attributed HT metamorphism to syn-magmatic deformation, later partially obliterated by amphibolite facies to low-grade metamorphism that occurred proximal to the sea floor. Caby (1995) associated amphibole-rich deformed gabbros and amphibole-bearing felsic veins to interaction with migrating seawater-derived fluids, also responsible for triggering shear zones formation in the gabbro. According to this hypothesis, the syn-kinematic partial melting of the sheared gabbro would have generated SiO_2-rich hydrous melts that fed the felsic veins. Tribuzio et al. (2019) conducted different chemical analyses on the sheared gabbro and the felsic veins, combining major and trace elements of both major minerals and whole rocks. They infer that

the chemically evolved melts that formed such veins were responsible for the HT metamorphism and that reactions between melt and gabbro led to metasomatism of the deformed gabbro. Noteworthy, they did not find any clear evidence of seawater-derived fluids triggering either the ductile shear zones or partial melting of the gabbro. However, recently, Nicollet et al. (2022) proposed two origins for the hydrous SiO_2-rich melts: both pervasive seawater-derived fluids and local exsolved magmatic fluids, derived from evolved hydrous silicate melts (infiltrated into an already cooled gabbro body).

The CO intrusive bodies were recently dated by Nicollet et al. (2022). U–Pb dating on zircons dated the magmatism to 161 ± 0.8 Ma in gabbro and 161.8 ± 1.7 Ma in albitite veins. U–Pb dating on monazite, xenotime, and titanite allowed the HT metamorphism to be constrained at 161.3 ± 4.0, 161.5 ± 2.4, and 158.4 ± 2.3 Ma. Previously, similar ages were constrained via U–Pb on zircons by Li et al. (2013) for the troctolite and albitite stocks (c. 165 Ma).

With the aim of providing new data on the metamorphic evolution of the CO, this paper focuses on the HP-LT metamorphic assemblages attributed to the Alpine orogeny and recognized in gabbroic samples from Rocca Remolon (eastern side of the CO) and the southwestern ridge of Le Chenaillet and in alkali syenite (i.e., albitite) samples from the Col du Gondran (both in the southwestern portion of the massif; Figure 1). Particular attention is given to the thermodynamic modelling of the Alpine pressure–temperature (P–T) evolution through isochemical phase diagrams and to the distinction of the HT metamorphism versus Alpine metamorphism.

2 | GEOLOGICAL SETTING AND LITHOSTRATIGRAPHY

The CO (also reported as Chenaillet massif or Montgenèvre ophiolitic complex in literature) crops out in the Western Alps, south of the villages of Montgenèvre and Claviere, crossing the French–Italian border over an area of about 25–30 km^2, at an altitude between 2000 and 2650 m a.s.l.

The CO is delimited to the north and to the south by late, high-angle faults that separate it from continental margin units (Barféty et al., 1995; Lagabrielle & Polino, 1988; Polino et al., 1983). It forms a klippe-like unit above the ophiolite-bearing blueschist-facies Lago Nero unit (e.g., Burroni et al., 2003; Polino & Lemoine, 1984), from which it is separated by a low-angle Alpine thrust fault. According to recent studies (Manatschal et al., 2011), this basal contact is deformed by large-scale west-vergent folds and Alpine reactivation of high-angle normal faults.

In contrast to the other surrounding meta-ophiolitic units of the Western Alps, the CO is believed to have never exceeded greenschist to prehnite-pumpellyite facies conditions during the Alpine metamorphism (Bertrand et al., 1982; Lewis & Smewing, 1980; Mével et al., 1978; Pusztaszeri, 1966).

The CO is mainly made of serpentinized peridotite (generally exposed in the eastern sector), mafic plutonic rocks, and overlying pillow lavas (in the western sector of the massif). Sedimentary rocks are scarce and comprise mainly breccias, originated by reworking of mafic and ultramafic rocks. Post-rift Late Jurassic to Cretaceous sedimentary rocks are absent, in contrast to the neighbouring oceanic units which comprise a large amount of post-rift meta-sedimentary rocks.

The mantle peridotite consists of strongly serpentinized lherzolite and harzburgite, with minor pyroxenite, dunite, and wehrlite (Bertrand et al., 1987; Figure 2a). Within the highly serpentinized mantle rocks, a thin sequence of layered troctolite and olivine-bearing gabbro occurs, less than 1 km in diameter and cross-cut by diorite, dolerite, and basalt dykes (Figure 2a,b). For this sequence, various hypotheses have been inferred: According to Costa and Caby (2001), the gabbroic rocks represent remnants of the oceanic lower crust, preserving a paleo-Moho with the mantle peridotite. On the other hand, Manatschal et al. (2011) proved that the mafic rocks are intrusive with respect to the mantle rocks, and Li et al. (2013) described these rocks as small magmatic bodies, whereas Chalot-Prat (2005) interpreted the gabbros as sill-like intrusions. Dolerite, diorite, and basalt dykes usually occur within sheared gabbro, close to high-angle normal faults. Albitite/alkali syenite bodies occur as dykes and sills at the serpentinized peridotite–gabbro boundary throughout the massif (Caby, 1995; Chalot-Prat, 2005; Figure 2a–c). The well-known volcanic sequence of the CO consists of lava flows, pillow basalts, pillow breccias, and hyaloclastites, with strong affinities with Mid-Oceanic Ridge Basalt series. Authors still do not agree on whether this volcanic sequence is linked to a single (Chalot-Prat, 2005) or several magmatic events (Li et al., 2013; Manatschal et al., 2011).

3 | SAMPLED ROCKS

Our petrological and petrographic investigation was focused on two lithologies: gabbro and albitite/alkali syenite (Figure 2b,c). Although we sampled a large number of lithologies from the area and observed them under both optical and scanning electron microscopes, these two kinds of rocks proved to be the most interesting and the ones with the most representative mineral

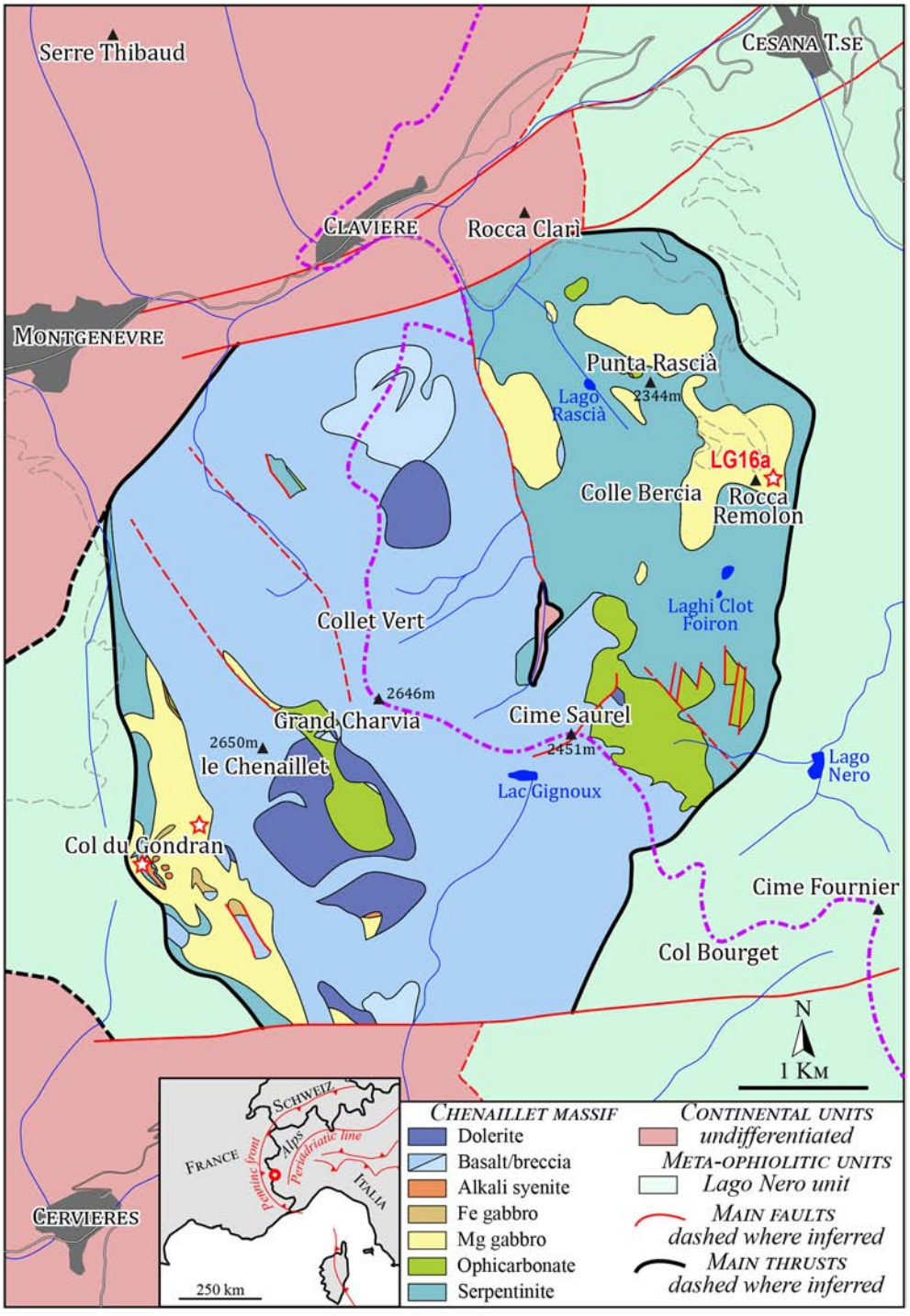

FIGURE 1 Schematic geological map of the Chenaillet Ophiolite, redrawn after Manatschal et al. (2011) and Chalot-Prat (2005). The red-white dot in the inset shows the position of the CO in the Western Alps, whereas the red-white stars in the geological map show the positions of the samples used for petrographic and mineral chemistry analyses. [Colour figure can be viewed at wileyonlinelibrary.com]

assemblages for the investigation of the Alpine metamorphic evolution. The basalts and pillow lavas of the CO did not prove to be useful for this kind of investigation, because they do not display either evidence of the HT deformation event occurring in the gabbro bodies or striking Alpine metamorphic peak mineral assemblages. Their main petrographic features are reported in Supporting Information S1.

Gabbro is coarse grained (Figure 2b) and has been subdivided into two types (according to Chalot-Prat, 2005): (i) olivine-bearing gabbro, with Mg-chlorite after pseudomorphosed olivine, albite over magmatic plagioclase, and minor preserved augite, and (ii) amphibole-bearing gabbro, with albite over magmatic plagioclase and abundant augite, partially replaced by different generations of late-magmatic amphiboles. Each gabbro body is made of smaller subbodies (from 1 to 10 m), surrounded by mylonitic, sheared boundaries (i.e., flaser gabbros) related to HT deformation during a late- to post-magmatic stage at granulite- and/or amphibolite-facies

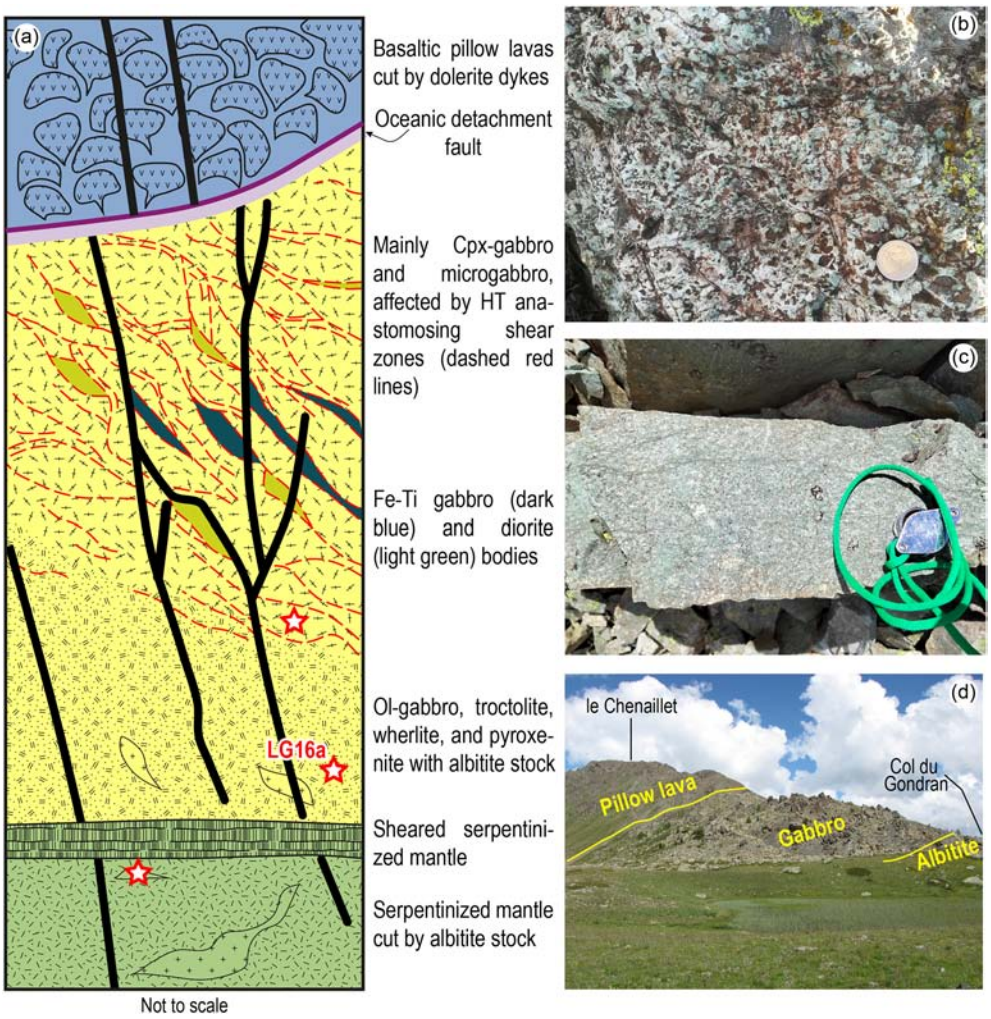

FIGURE 2 (a) Simplified stratigraphic section of the Chenaillet ophiolite, redrawn after Costa and Caby (2001); the red-white stars show the lithologies sampled for analyses; (b) gabbro outcrop of Rocca Remolon, characterized by coarse-grained texture and minor sheared flaser gabbro; (c) albitite/alkali syenite outcrop at the Col du Gondran; and (d) landscape picture of the Col du Gondran area and its geology. [Colour figure can be viewed at wileyonlinelibrary.com]

conditions (Caby, 1995; Mével et al., 1978; Nicollet et al., 2022; Tribuzio et al., 2019). Gabbros have been sampled both on the eastern and western sides of the CO; among them, the gabbro from Rocca Remolon (southeast of Punta Rascià; 44°55′14.62″N 6°47′22.42″E) proved to be the most interesting. Albitite has been thoroughly studied by Martin (1984) and displays an apparent trivial composition with a large amount of albite (up to 90%), minor LT amphiboles and fine-grained omphacite (responsible for the light-green and whitish colour; Figure 2c), large zircon crystals, allanite, and apatite. Albitite has been sampled at the Col du Gondran (Figure 2d), where a large albitite sill is exposed at the peridotite-gabbro boundary (44°53′40.03″N 6°43′42.35″E).

4 | METHODS

4.1 | Petrography and mineral chemistry

A Scanning Electron Microscope (JEOL JSM-IT300LV) equipped with an energy-dispersive X-ray spectrometer, with an SDD (a silicon drift detector from Oxford Instruments), hosted at the Dipartimento di Scienze della Terra of the Università degli Studi di Torino, was used for the determination of major elements. The experimental conditions include the following: accelerating voltage 15 kV, counting time 50 s, process time 5 μs, and a working distance of 10 mm. The measurements were conducted under high vacuum conditions. The energy-dispersive X-ray spectrometer-acquired spectra were corrected and calibrated both in energy and in intensity thanks to measurements performed on cobalt standard introduced in the vacuum chamber with the samples. The Microanalysis Suite Oxford INCA Energy 300, which enables spectra visualization and elements recognition, was employed. A ZAF data reduction program was used for spectra quantification. The resulting full quantitative analyses were performed, using natural oxides and silicates from Astimex Scientific Limited, as standards. Potassic white micas have been classified as muscovite or phengite according to their Altot/Si ratio (i.e., muscovite: $Al_{tot} > 5.00$, $Si < 3.30$; phengite: $Al_{tot} < 5.00$, $Si > 3.30$). XMg of pumpellyite is defined as $Mg/(Mg + Fe^{2+})$. XZo in

epidote-group minerals is defined as $Al/(Al + Fe^{3+})$. Representative analyses of mineral composition are reported in Supporting Information S1. Structural formulae have been calculated using algorithms in XMapTools (Lanari et al., 2019 and references therein) on the basis of six oxygens for clinopyroxene, eight oxygens for lawsonite and albite, 11 oxygens for white mica, 14 oxygens for chlorite, 23 oxygens for amphiboles, 24 oxygens for prehnite, 24.5 oxygens for pumpellyite, and 25 oxygens for epidote. Mineral abbreviations are according to Whitney and Evans (2010) (Wm = potassic white mica).

High-resolution multispectral maps of the thin sections used for deriving the effective bulk composition of the investigated sample were obtained using the same Scanning Electron Microscope with Energy Dispersive X-ray Spectroscopy (SEM-EDS) instrument. Operative conditions used for mapping the entire thin section were the following: 15 kV accelerating voltage, 5 nA probe current, 1 μs EDS process time, 10^5 cnts/s, 2.5 μm point step, and 1 ms dwell time. The row data were processed using the MultiSpec© software to obtain the modal composition.

5 | PETROGRAPHIC FEATURES AND MINERAL CHEMISTRY OF ANALYSED SAMPLES

This section summarizes the petrographic and mineral chemical features of two types of rocks: gabbro and albitite (i.e., alkali syenite). Although only a gabbro sample has been used for thermodynamic modelling, also the main features of the albitite are reported, because this lithology proves to be useful to constrain the Alpine metamorphism experienced by this unit. Other lithologies from the area (e.g., basalts and diorites) were sampled and analysed, but they proved to be less explicative and less reactive during the Alpine metamorphic evolution. A brief petrographic description of the basalt and pillow lava is provided in Supporting Information S1.

Gabbro

Gabbro still preserves the original, coarse-grained, magmatic texture (Figure 2b). Mg-gabbros are characterized by two main micro-structural domains: (ex-)plagioclase sites and clinopyroxene sites (Figures 3 and 4). They are made of Ca-clinopyroxene (32–36%) + albite (23–26%) + HT Ca-amphiboles (11–15%) + Mg-chlorite (7–8%) + pumpellyite (4–9%) + LT Ca-amphiboles (4–5%) + lawsonite (1–6%) + epidote (0–5%) + titanite (0.5%) + prehnite (0–5%) ± white mica (0.5–6%) and minor quartz, rutile, and ilmenite (<0.5% in total).

Plagioclase sites, usually rounded in shape, are now completely replaced by fine-grained aggregates (pseudomorphoses) of albite, pumpellyite, and lawsonite, with the local occurrence of sericitic white mica and epidote (Figure 3a,b). Albite represents the majority of the site, whereas lawsonite occurs in small (up to 100 μm) anhedral crystals (Figure 4a) without any preferential orientation (Figure 4e,f). Pumpellyite, 50 μm in length, usually grows over (or in association with) lawsonite, wrapped by albite and oligoclase (Figure 4e). White mica occurs only in some of the samples and seems to grow coeval with pumpellyite over lawsonite (Figure 4e). Locally, epidote grows together with white mica as saussurite aggregates after lawsonite. Prehnite may be associated with epidote in these sites, but more often it occurs in thin veins (Figure 3c,d), locally with epidote.

Clinopyroxene sites are composed of preserved magmatic clinopyroxene, partially replaced by large HT Ca-amphiboles (Figure 3a,b). HT Ca-amphiboles grow in two micro-structural sites with respect to clinopyroxenes: They can form large rims, up to 200–300 μm (Figures 3a,b and 4a,b), or can grow as exsolutions inside clinopyroxene crystals (Figures 3b and 4c,d). The clinopyroxene is often rimmed by LT Ca-amphiboles and Mg-chlorite (Figures 3b and 4a,b). This assemblage can also occur in thin veins (Figure 3c) and large pseudomorphs after completely retrogressed olivine, as observed also by Chalot-Prat (2005) (Figures 3c,d and 4c).

Titanite crystals (usually occurring in the proximity of clinopyroxene sites) grow over both magmatic ilmenite. Rutile, although very rare and usually smaller than 10 μm (Figure 3d), grows intimately associated with titanite and has been ascribed to the peak mineral assemblage, because it usually represents the Ti-bearing mineral phase stable at higher pressures (see Angiboust & Harlov, 2017). A summary of the blastesis/deformation relationships is presented in Table 1.

In Mg-gabbros, clinopyroxene plots in the Q vertex of the Morimoto (1988), with augitic and diopsidic compositions (Figure 5a,b). A confined linear correlation between the amount of Al in the M1 site and the XNa, defined as $Na/(Na + Ca)$, is observed (Figure 5c). Ca-amphiboles have been classified based on Hawthorne et al. (2012) and Leake et al. (1997). Based on Na (a.p.f.u.) occurrence in site B (Figure 5d), Na- and Ca/Na-amphiboles have not been found, whereas Ca-amphiboles (Figure 5d,e) occur as HT amphibole (with zoning composition from pargasite to edenite/hornblende) and LT amphibole (actinolite s.l.). Na + K in site A versus Al^{IV} diagram mostly points to compositions ranging from pargasite to hornblende, with only local edenite and tschermakite compositions (Figure 5e). XMg versus Si diagram (Figure 5f) permits constraining amphiboles to Mg-rich

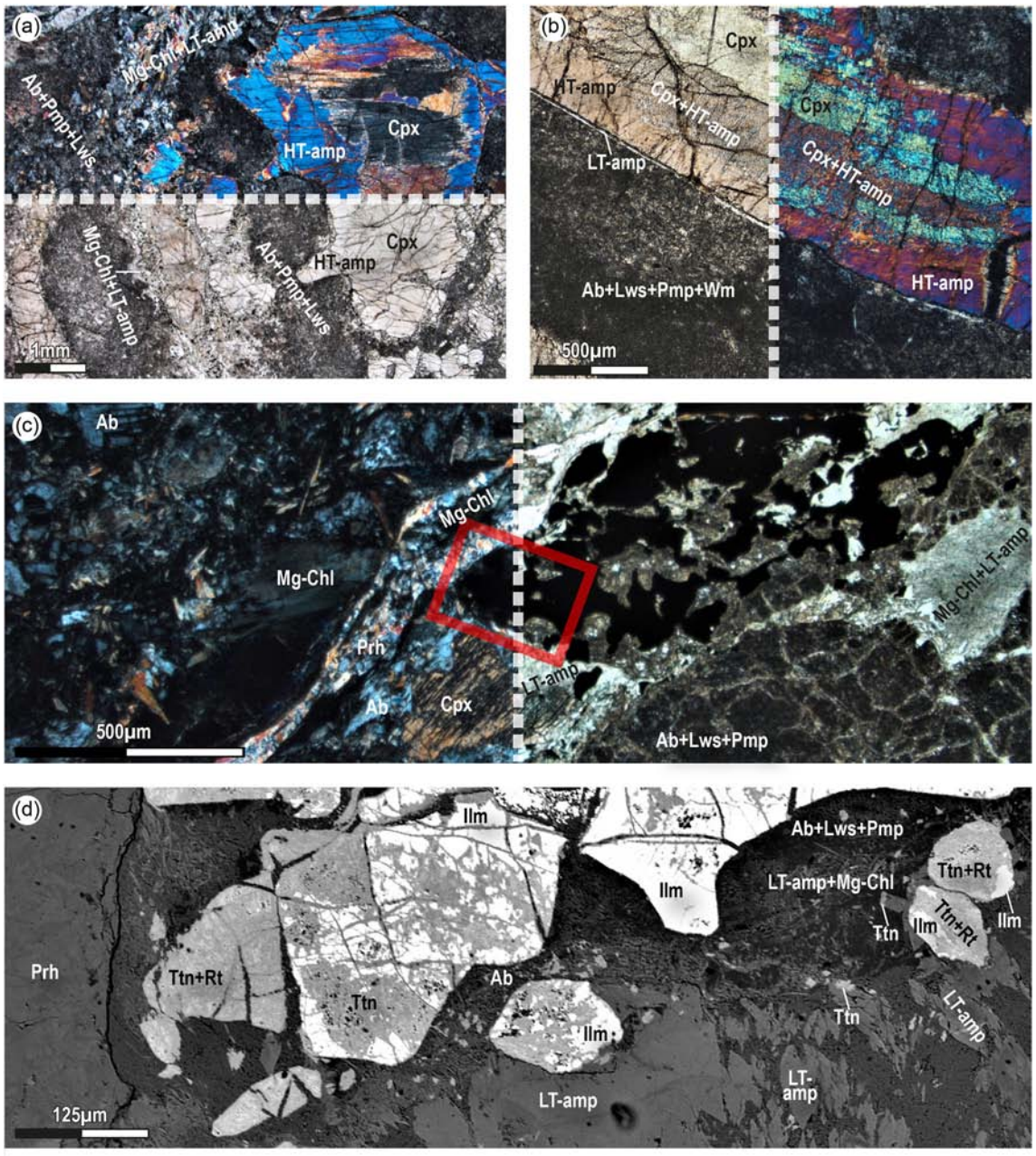

FIGURE 3 Representative microstructures and mineral assemblages of the gabbro from the CO. (a) Typical coarse-grained texture of the gabbro, characterized by two main micro-structural domains: (ex-)plagioclase sites (now made of lawsonite + albite + pumpellyite) and clinopyroxene sites (with magmatic clinopyroxene preserved and rims and patches of HT-amphiboles). Locally, Mg-chlorite + LT-amphibole completely replace retrogressed olivine (upper-part crossed polarized light, XPL, lower part plain polarized light, PPL); (b) large clinopyroxene crystals characterized by HT-amphibole growing both at rims and in patches inside the clinopyroxene, whereas LT-amphibole grows as thin rims all around clinopyroxene and HT-amphiboles. Locally, the ex-plagioclase sites can be characterized by fine-grained white mica (left-side PPL, right-side XPL); (c) complex fine-grained microstructure characterized by ex-olivine crystals (now completely replaced by Mg-chlorite + LT-amphibole), small clinopyroxene crystals, fine-grained ex-plagioclase sites (now made of albite + lawsonite + pumpellyite), and a prehnite vein (right-side PPL, left-side XPL). The red polygon shows the position of the inset in (d); and (d) inset of Figure 3c seen under SEM (backscattered electron image). Note that the prehnite vein is on the left side of the figure and the idioblastic, small, LT-amphibole crystals are on the right-side. [Colour figure can be viewed at wileyonlinelibrary.com]

compositions. LT amphibole occurs both as actinolite (s.s.) and tremolite (XMg > 0.90). White mica displays shifting (zoning) compositions (Figure 6a), from muscovite (Si < 3.25 a.p.f.u.) up to phengite (Si from 3.25 to 3.40 a.p.f.u.). Pumpellyite, enriched in Al, has XMg ranging from 0.60 to 0.80 (Figure 6b). The original

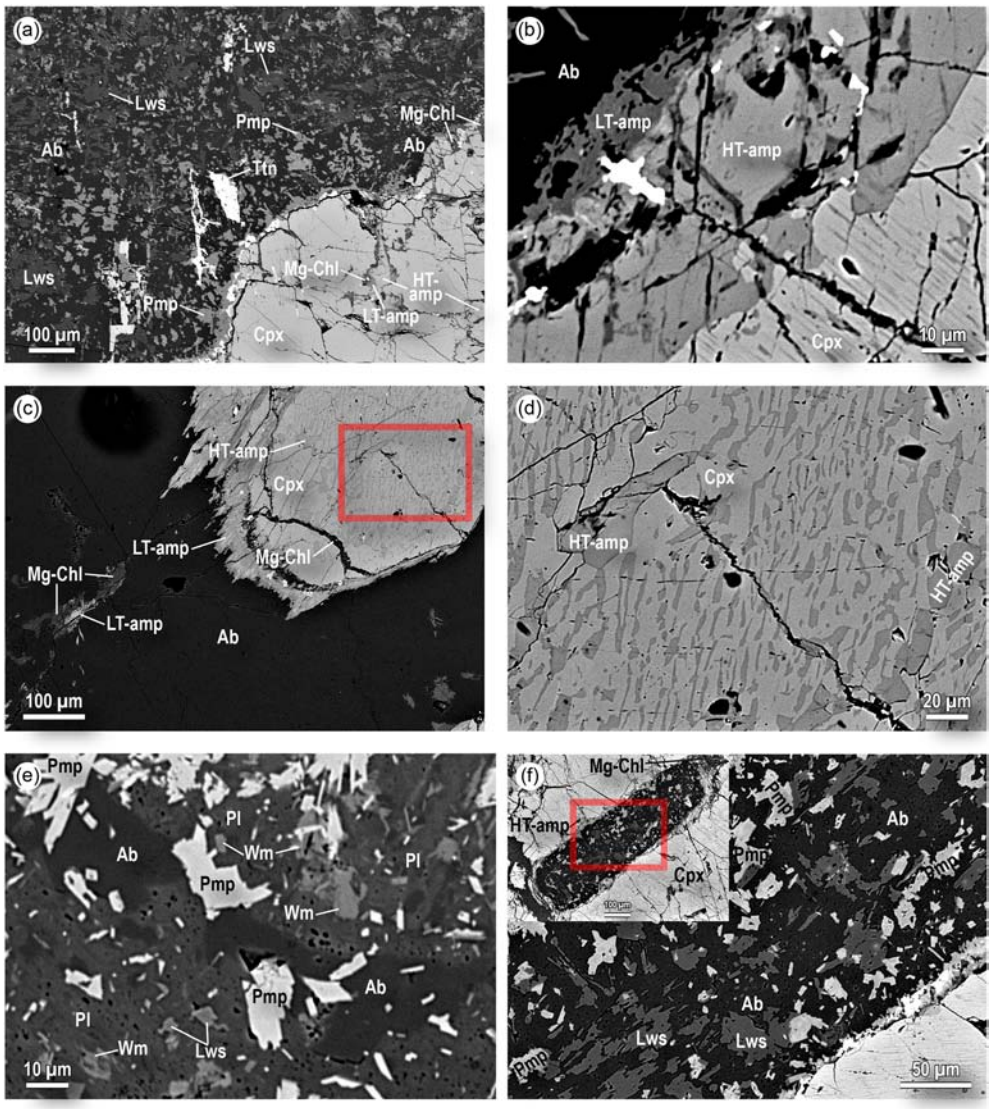

FIGURE 4 Representative microstructures and mineral assemblages under SEM (backscattered electron image images). (a) Typical gabbro texture characterized by ex-plagioclase site and clinopyroxene site. Lawsonite, occurring in the plagioclase site, occurs in small crystals (up to 100 μm), partially replaced by pumpellyite. Clinopyroxenes are usually fractured with growth of Mg-chlorite and LT-amphibole along fractures; (b) detail of the edge of a magmatic clinopyroxene, rimmed by HT-amphibole (approximately 50 μm) and then by thin LT-amphibole (10 μm); (c) magmatic clinopyroxene rimmed by LT-amphibole, with Mg-chlorite growing in fractures and HT-amphibole patches. Note the aggregate of Mg-chlorite + LT-amphibole over completely replaced olivine; (d) inset referred to the red polygon in (c), showing the intergrowths of HT-amphibole inside the clinopyroxene; (e) ex-plagioclase site made of small lawsonite crystals (<10 μm), partially overgrown by pumpellyite and small white mica flakes, within a plagioclase matrix partially preserving HT-plagioclase (Pl) and only locally albite replacement (inner and darker portion); and (f) ex-plagioclase crystal preserving its idioblastic shape (in the inset), now completely retrogressed by lawsonite, pumpellyite, and albite. Note that the pumpellyite crystals are partially replacing earlier lawsonite. [Colour figure can be viewed at wileyonlinelibrary.com]

magmatic plagioclase is usually replaced by albite; however, rare relics of less retrogressed, Ca-richer plagioclase can still be found, with compositions up to labradorite (Figure 6c). Epidote group minerals display a very large range of compositions, from 100% zoisite to 85% epidote (s.s.; Figure 6d). Chlorite, occurring both in veins and after olivine crystals, has Mg-rich compositions with XMg values mostly in the range 0.73–0.75.

5.1 | Albitite/alkali syenite

Albitite displays a typical ophitic texture, with large amounts of albite, intergrown with minor clinopyroxene and LT Ca-amphibole. It is made of albite (up to 90%), clinopyroxene, Ca-amphibole, titanite, large zircon crystals, allanite, and apatite. Clinopyroxene occurs in two micro-structural sites: as large crystals, up to 400 μm

TABLE 1 Blastesis/deformation relationships of the gabbroic rocks from the Chenaillet Ophiolite.

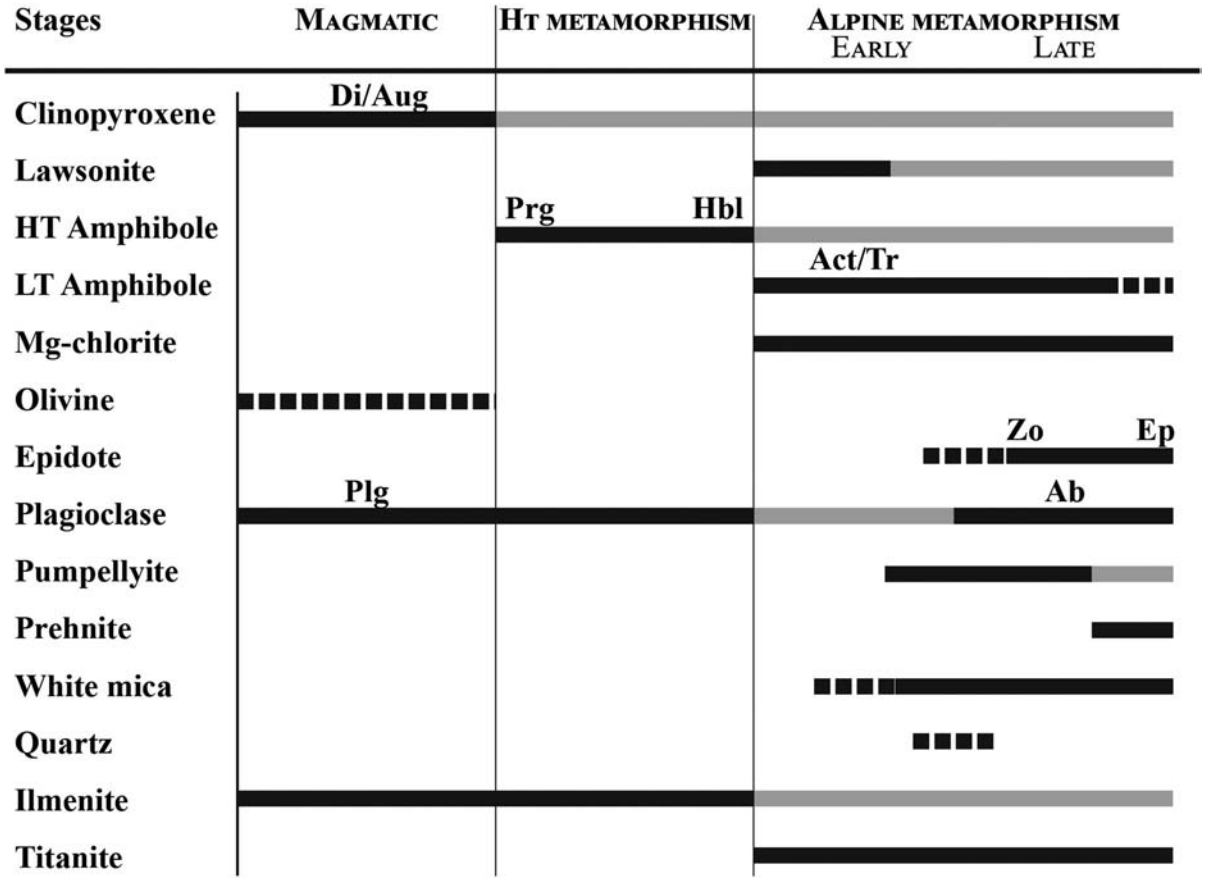

Note: Black lines are for stable mineral phases in equilibrium with the mineral assemblage during a precise time in their evolution (dashed were inferred or very scarce). Grey lines are for metastable mineral phases still occurring in the rocks but no more at the equilibrium with the mineral assemblage.

(Figure 7a), intergrown with large albite crystals, or as aggregates of small acicular crystals (Figure 7b), usually smaller than 100 μm, grown along the albite grain boundaries. Also, Ca-amphibole grows in two microstructural sites: as rims around clinopyroxene or as large euhedral crystals, dispersed in the "albitic matrix" of the rock.

In the albitites, clinopyroxene crystals are zoned from Ca-rich to Ca-Na-rich compositions (Figure 5a). Magmatic relicts plot in the diopside-hedenbergite fields of Morimoto (1988; Figure 5b), and a second generation of clinopyroxene plots well within the Ca-Na clinopyroxene field, with compositions ranging from aegirine-augite to omphacite (Figure 5b). This second generation of clinopyroxene has XNa values (i.e., Na/Na + Ca a.p.f.u.) ranging from 0.20 to 0.64 and Al in the M1 site linearly increasing with increasing XNa (Figure 5c). Amphiboles plot in the Ca-amphiboles field of Hawthorne et al. (2012; Figure 5d,e), with low Al_{IV} values. They show compositions in the actinolite (s.s.) field, with a large range of XMg from 0.4 to 0.7, increasing with the increasing amount of Si (Figure 5f). Albite is compositionally pure, with no Ca content (Figure 6c).

6 | THERMODYNAMIC MODELLING

A P–T isochemical phase diagram was calculated for the gabbro sample LG16a. This specific gabbro sample was selected for the thermodynamic modelling because it preserves very well the Alpine peak mineral assemblage (e.g., it contains 6% of lawsonite) and it is devoid of white mica and epidote (both <0.5%), thus allowing to simplify the system by neglecting K_2O and Fe_2O_3. Isochemical phase diagrams have not been modelled for albitites because of their high variance mineral assemblage, although the newly reported occurrence of metamorphic Ca-Na clinopyroxenes provides important constraints on the metamorphic evolution of these rocks (see below). The bulk rock composition of sample LG16a was calculated by combining the mineral proportions obtained

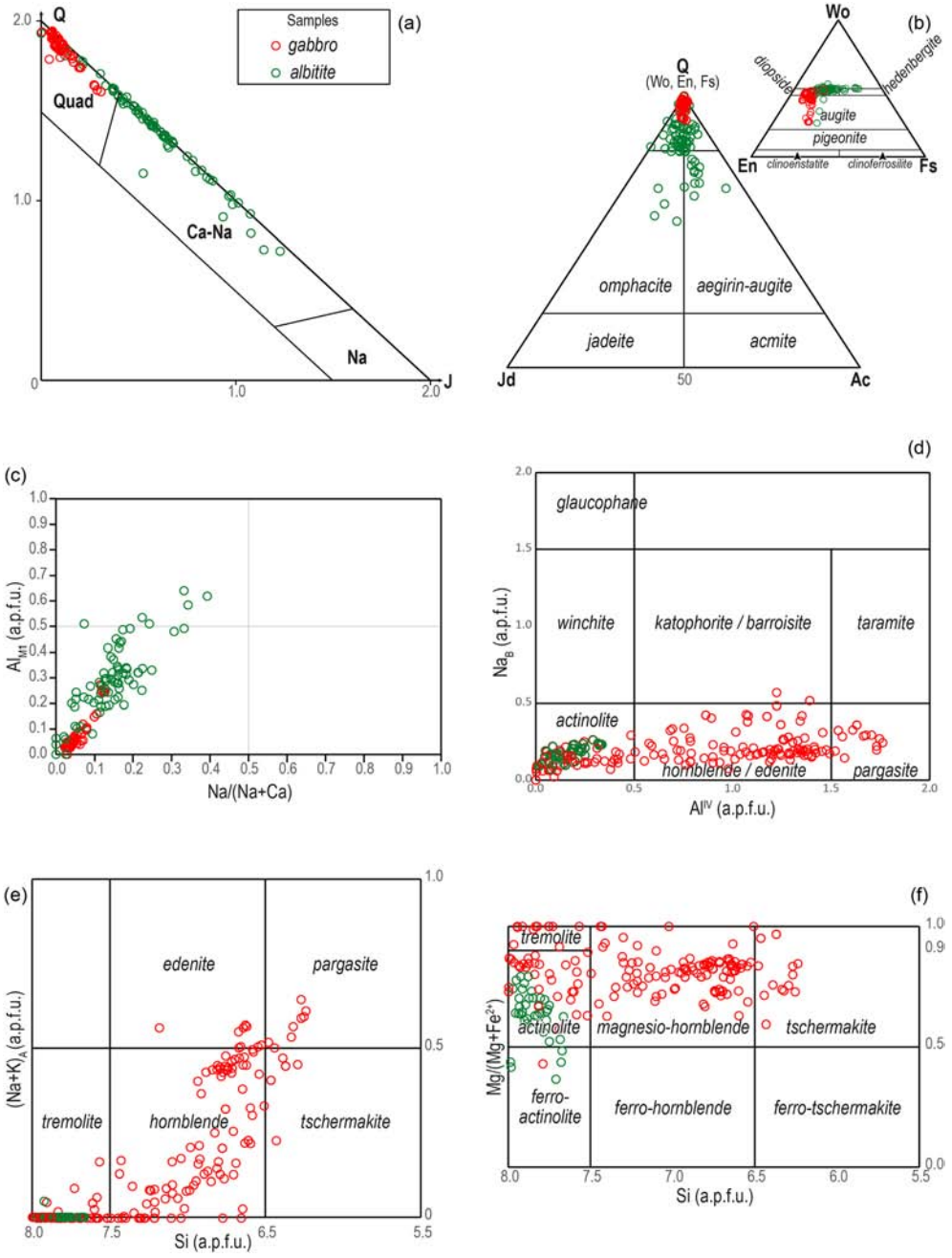

FIGURE 5 Mineral chemistry and classification diagrams for gabbro and albitite samples. (a) Morimoto (1988) pyroxene diagram QUAD: Ca-Mg-Fe pyroxenes, J: 2Na, Q: Ca-Mg-Fe^{2+}; (b) Morimoto (1988) pyroxene diagram; the Q vertex for magmatic clinopyroxene is also reported on the right. Note the occurrence of metamorphic Na-Ca clinopyroxene in the albitite and the shifting composition of magmatic clinopyroxene, between diopside and augite composition; (c) Al amount (a.p.f.u.) in the M1 site versus XNa (Na/Na + Ca), showing a linear correlation both in the magmatic clinopyroxenes in the gabbro and in the albitite; (d) amphiboles composition plotted in the Hawthorne et al. (2012) diagram NaB versus Al^{IV}. Na-amphibole has not been found, whereas Ca-amphiboles can be distinguished between LT (low Al content) and HT (high Al content); (e) amphiboles composition in the Hawthorne et al. (2012) diagram Na + K versus Al^{IV}. Although the amphiboles in the gabbro display variable compositions, from pargasite to hornblende and tremolite, the amphiboles in the albitite plot only in the tremolite (LT) field; and (f) XMg versus Si (a.p.f.u.) diagram for amphiboles: Although LT-amphiboles from the albitite plot in the actinolite-tremolite fields, both LT and HT amphiboles from the gabbro display higher XMg values. [Colour figure can be viewed at wileyonlinelibrary.com]

from the quantitative modal estimate of SEM-EDS multi-spectral maps, with single-point analyses acquired at SEM-EDS (all reported in Figure 8).

The P–T pseudosection was calculated in the system NCFMASTH (Na_2O-CaO-FeO-MgO-Al_2O_3-SiO_2-TiO_2-H_2O) using Perple_X 6.9.1 (Connolly, 1990, 2005, 2009),

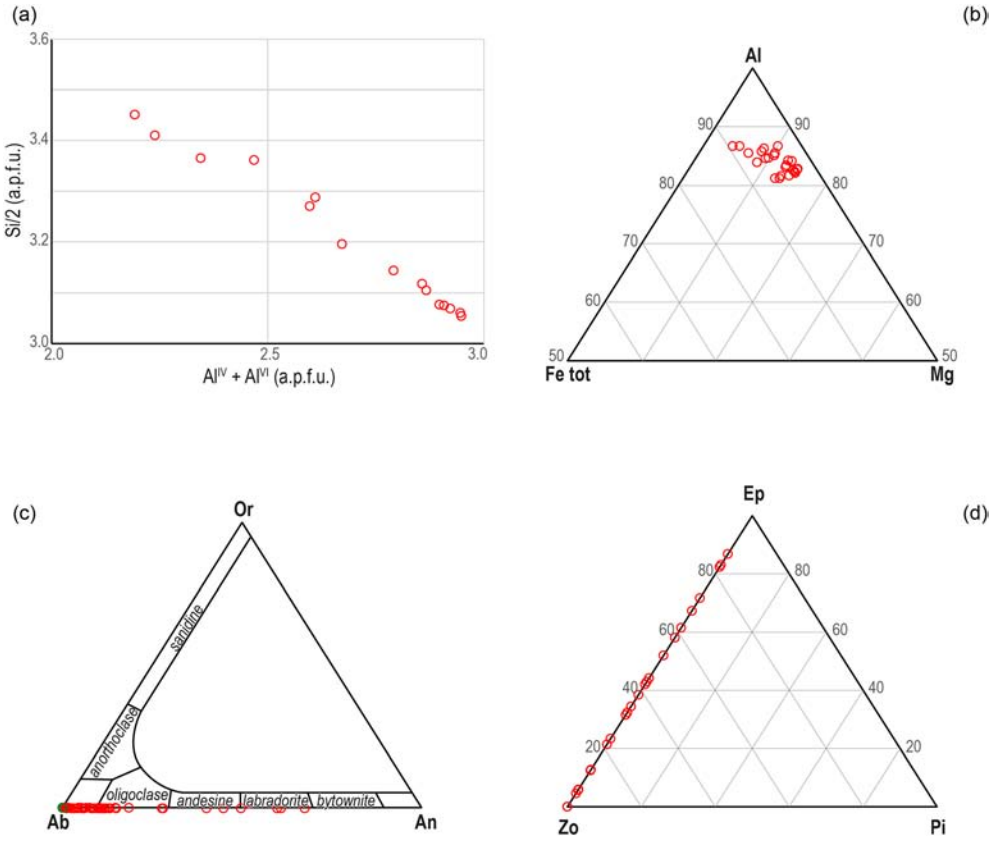

FIGURE 6 Mineral chemistry and classification diagrams for gabbro and albitite samples. (a) White mica composition plotted in the Si versus ($Al^{IV} + Al^{VI}$) diagram. Even though no distinct generations can be distinguished, compositions shift from muscovite to phengite; (b) pumpellyite ternary diagram (Mg-Al-Fe_{tot}), showing a single generation of pumpellyite occurring in the gabbro samples; (c) plagioclase classification diagram (after Deer et al., 1997). Although plagioclase from albitite plots only in the albite field, plagioclase from the gabbro plots in a larger range from albite to labradorite; and (d) epidote group minerals occur only in the gabbro and display all kind of compositions, from 100% to 15% zoisite. [Colour figure can be viewed at wileyonlinelibrary.com]

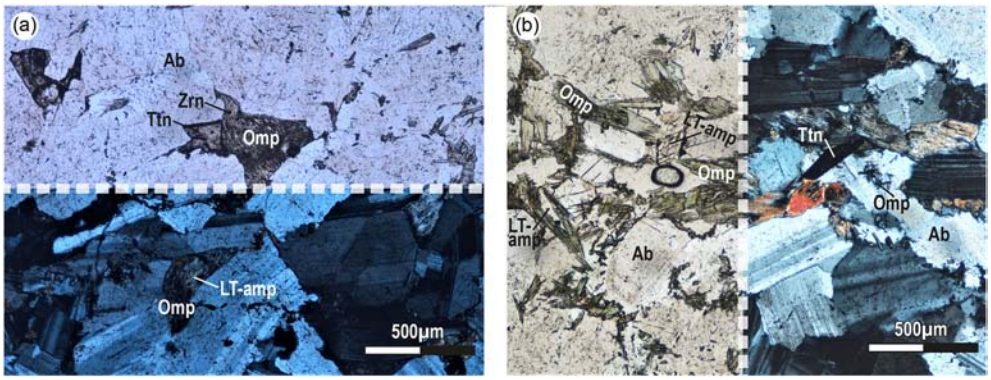

FIGURE 7 Representative microstructures and mineral assemblage of albitite seen under optical microscope. (a) Large omphacite crystal intergrown with albite and titanite (upper part plain polarized light, lower part crossed polarized light); and (b) small acicular crystals of omphacite growing along albite grain boundaries, partially replaced by LT-amphiboles. [Colour figure can be viewed at wileyonlinelibrary.com]

the internally consistent thermodynamic database of Holland and Powell (2011) (ds62), and the equation of state for H_2O of Holland and Powell (1998). Fluid saturated conditions were assumed, and the fluid was considered as pure H_2O ($aH_2O = 1$). The fluid saturation assumption was validated by calculating two P-M(H_2O) (mol%)

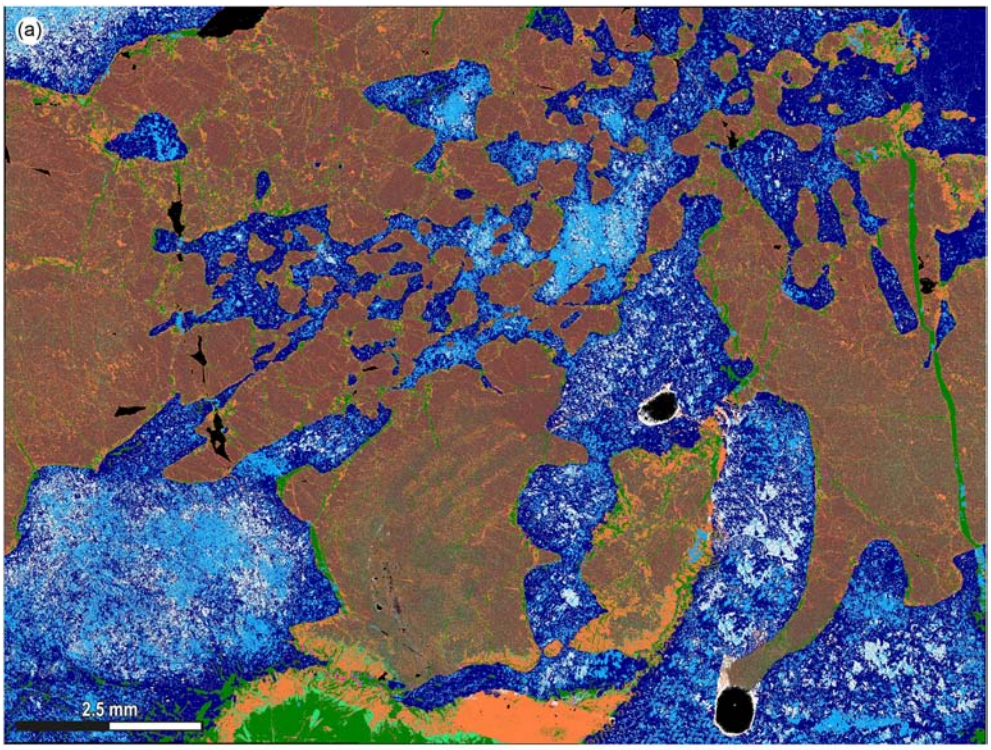

(b)

LG16a	SiO_2	Al_2O_3	MgO	FeO	CaO	Na_2O	K_2O	TiO_2	Total
Mol%	52.36	5.58	17.16	3.73	18.80	2.22	---	0.15	100.00
	Ab	Cpx	HT Amp	LT Amp	Pmp	Chl	Lws	Ttn	Total
Mode%	26.05	35.78	11.49	4.27	8.92	6.97	5.64	0.56	99.68

FIGURE 8 Gabbro sample LG16a used for thermodynamic modelling. (a) Processed X-ray map of the modelled sample; and (b) bulk rock composition (mol %) and mode % of the main minerals of the modelled sample. [Colour figure can be viewed at wileyonlinelibrary.com]

isochemical phase diagrams at T = 300°C and T = 350°C, available in Figure S1a,b. MnO and K_2O were neglected because Mn- and K-bearing phases are lacking. Fe^{3+} was neglected because Fe^{3+}-rich oxides are absent, and the amount of Fe^{3+} in the analysed minerals is very low. Nevertheless, the effects of Fe^{+3} on the stability of the observed peak mineral assemblage were investigated by calculating two P-X(Fe_2O_3) isochemical phase diagrams at T = 300°C and T = 350°C, reported in Figure S1c,d. These calculations demonstrate that the observed peak assemblage is limited to X(Fe_2O_3) < 0.5 and that its stability field is shifted towards progressively higher pressures with the increase of the oxidation state of the system. Hence, the assumption that all Fe is bivalent implies that the estimated peak pressures are minimum pressures.

The following solid solution models were used: biotite, chlorite, garnet (White et al., 2014), clinopyroxene (Green et al., 2007), amphibole (Green et al., 2016), feldspar (Fuhrman & Lindsley, 1988), and epidote (Holland & Powell, 1998). An ideal pumpellyite solution model has been used, assuming Fe-Mg occupies two octahedral (M1) sites and Al-Fe^3 occupies five (M2) sites. Quartz, lawsonite, talc, and kyanite were considered as pure phases. The P–T evolution for the gabbro sample was constrained based on the predicted stability fields of the observed assemblages, as well as the predicted modal (vol%) amounts of each mineral phase.

The isochemical phase diagram was modelled in a wide range of P–T conditions (250–700°C and 1–15 kbar). The unfractionated bulk composition (i.e., the measured bulk composition reported in Figure 8b, obtained as described in Section 4) was used for the modelling, thus including both the magmatic and HT-related mineral relicts (i.e., clinopyroxene and HT Ca-amphibole, respectively). The same approach was used in other studies (e.g., Bucher et al., 2005; Bucher & Grapes, 2009) on similar lithologies from other meta-ophiolitic sequences of the Western Alps. To test the reliability of the used bulk rock composition, the modelled sample was further investigated by inductively coupled plasma-mass spectrometry (ICP-MS) conventional geochemical analysis. Both bulk compositions were then compared with other bulk rock compositions of (meta-)gabbro samples from the CO (Bertrand et al., 1982; Chalot-Prat, 2005; Costa & Caby, 2001) and from similar geological setting either in

the Alps (Bocchio et al., 2000; Bucher & Grapes, 2009) or beyond (Montanini et al., 2008; Shi et al., 2008) (Figure 9a,b).

The results of the modelling are shown in Figure 10a,b; geotherms typical of subduction settings (Agard, 2021; Agard et al., 2001), ranging from 7°C/km to 25°C/km, are shown in the same figure because they are useful for interpreting the P–T evolution of the studied rocks. The isochemical phase diagrams in Figure 10a,b are matched with pie charts (Figure 10c) for the predicted volume% of each mineral at specific P–T conditions (yellow dots in Figure 10a,b); Figure 9d illustrates the variation in mineral modes along a hypothetical isothermal exhumation path (marked by yellow dots in Figure 10a,b). Isochemical phase diagrams with the predicted volume% of the main Alpine mineral phases are reported in Figure S2.

The modelled isochemical phase diagram is dominated by tri- and quadri-variant fields (Figures 10a,b), with minor narrow divariant fields. The lawsonite-epidote transition is marked by a discontinuous reaction (yellow curve in Figure 10b) with a steep positive slope. Pumpellyite is predicted in a limited sector of the phase diagram, for T < 400°C and P between 11 and 3 kbar (lilac curve). A clinopyroxene with diopsidic composition (Cpx) is predicted to be stable in all the investigated P–T range, and a second clinopyroxene (Omp) is predicted at extremely LTs (T < 300°C and P > 7 kbar). LT Ca-amphibole, mainly actinolite (Amp1), is predicted to be stable in almost in every field of the phase diagram (green curve), whereas at T > 500°C, a second, pargasitic amphibole (Amp2) is predicted to occur (dark green curve).

The original magmatic mineral assemblage, already affected by HT metamorphism, is modelled by a small field at P < 2 kbar and T > 700°C (lower right corner of Figure 10a,b), consistently with the results of previous studies (e.g., Nicollet et al., 2022). This field is characterized by diopsidic/augitic clinopyroxene, pargasitic amphibole, ilmenite, and plagioclase.

The current mineral assemblage is the result of a complex sequence of metamorphic assemblages developed during decompression from P > 11 kbar to P < 3 kbar at a nearly constant temperature of around 350–300°C:

- At peak P–T conditions, the studied gabbro still contained abundant magmatic clinopyroxene (Cpx: 60% in absolute volume), only partially replaced by actinolite (Amp1: 19.5% in absolute volume) + chlorite (3%); lawsonite (17%) grew at the expenses of magmatic plagioclase, and titanite (0.5%) completely replaced magmatic ilmenite. This assemblage (Cpx + Amp1 + Chl + Lws + Ttn) allows predicting a range of P–T conditions from a minimum of 9 kbar and 350°C to a maximum of 15 kbar and 450°C, which are compatible with a geothermal gradient of 8–10°C/km (Figure 10a,b).
- At about 9 kbar and 350°C (i.e., 12°C/km geothermal gradient), the breakdown of lawsonite occurred, which was retrogressed mainly to pumpellyite (22% in

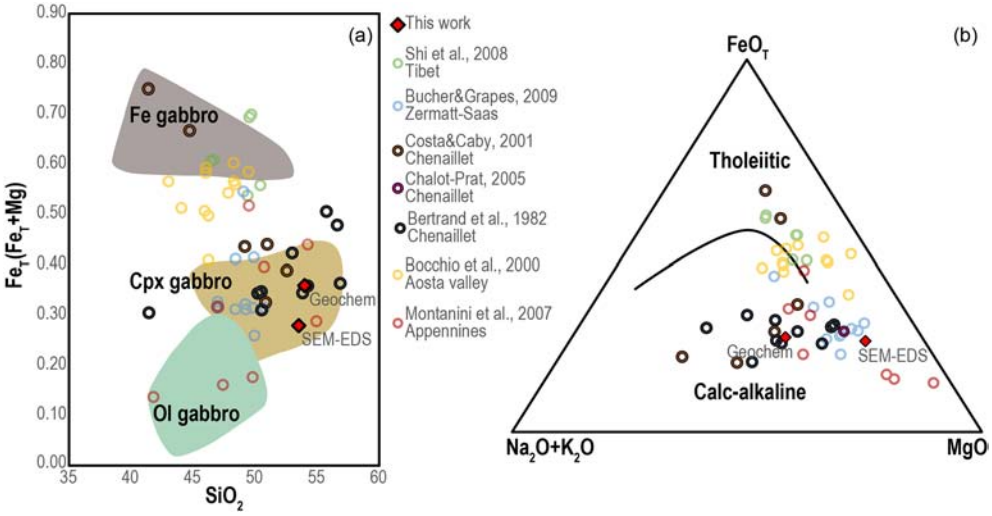

FIGURE 9 (a, b) Bulk-rock composition diagrams (wt%) comparing the bulk rock composition of the gabbro sample LG16a used for thermodynamic modelling with other gabbros from the same area, the Alps and other geological setting. (a) Fe_{tot} versus SiO_2 diagram; (b) $Na_2O + K_2O$-MgO-Fe_{tot} ternary diagram. In both diagrams, SEM-EDS label stands for "calculated by combining the mineral proportions obtained from the quantitative modal estimate of SEM-EDS multispectral maps, with single-point analyses acquired at SEM-EDS", whereas "Geochem" label stands for "acquired with ICP-MS conventional geochemistry." [Colour figure can be viewed at wileyonlinelibrary.com]

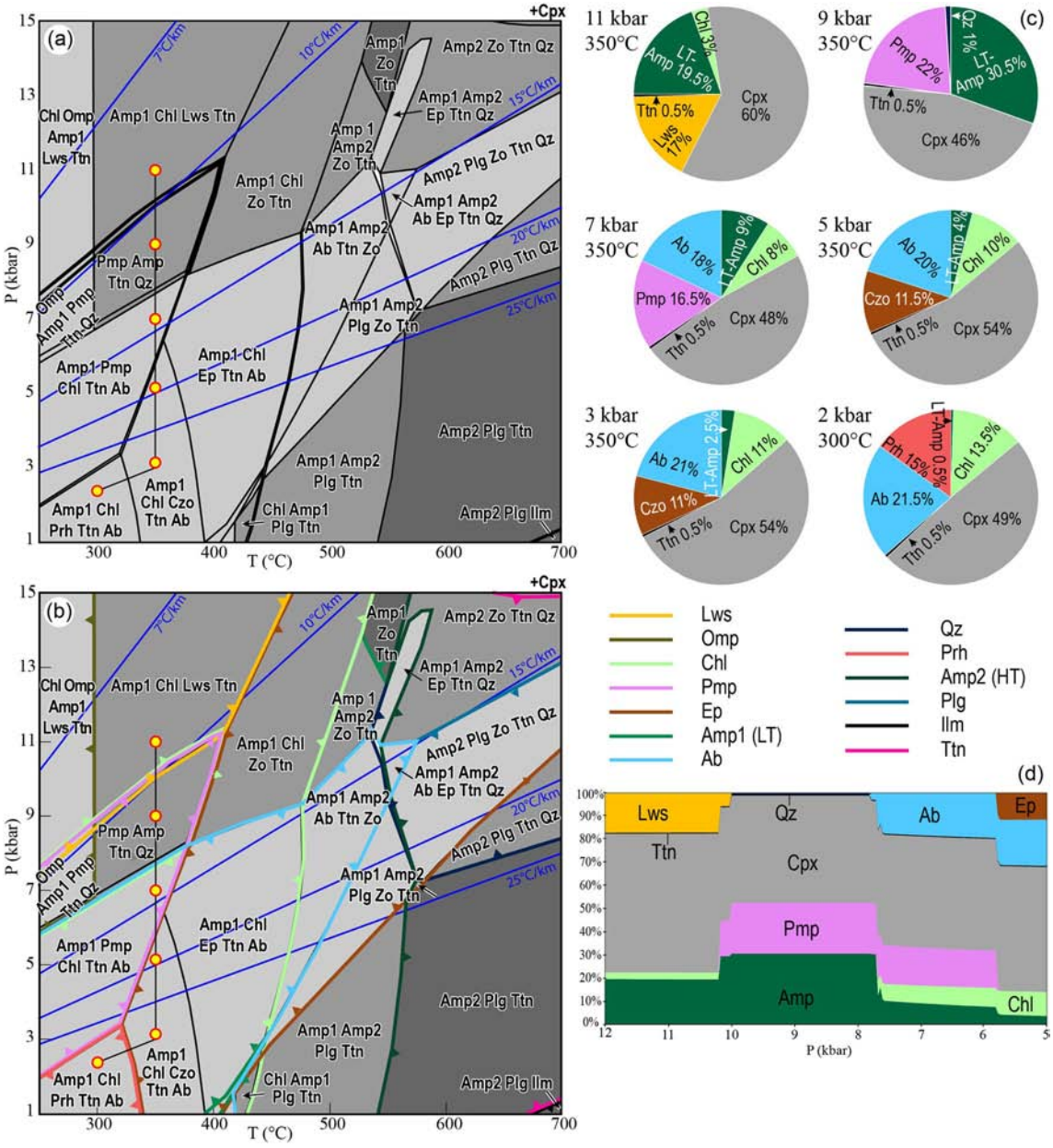

FIGURE 10 (a, b) P–T isochemical phase diagrams calculated for the modelled sample LG16a, using the bulk rock composition reported in Figure 8b. Yellow dots correspond to P–T conditions at which pie charts in Figure 9c were calculated. The phase-in and phase-out boundaries for the main minerals are reported in (b); colour coded according to legend on the right; (c) pie charts for predicted volume% of each mineral phase, calculated at the specific P–T conditions reported by the yellow dots in (a) and (b); and (d) variation of mineral modes along a hypothetical isothermal exhumation path, marked by yellow dots in (a) and (b). [Colour figure can be viewed at wileyonlinelibrary.com]

absolute volume). At this stage, chlorite was no longer stable and was partially replaced mainly by actinolite (30.5%) and very low amounts of quartz (1%), which grew also at the expense of HT Ca-amphibole and diopsidic clinopyroxene.

- At approximately 7 kbar, 350°C (i.e., 15°C/km geothermal gradient), albite grew (18% in absolute volume) in the plagioclase domains and partially replaced pumpellyite (16.5%). At this stage, chlorite started growing again (8%), partially over actinolite and clinopyroxene (48%).
- At 5 kbar (i.e., 20°C/km geothermal gradient), pumpellyite was no longer stable and was replaced by clinozoisite (11.5% in absolute volume), which also overgrew the metastable preserved lawsonite relics. The amount of stable LT-amphibole decreased (to 4%),

whereas albite and chlorite increased (to 20% and 10%, respectively). At 3 kbar, this trend continued, with decreasing amount of actinolite (2.5%) and (slightly) increasing amounts of albite (21%) and chlorite (11%), whereas clinozoisite amount remained unchanged (11%).
- Finally, along a 25–30°C/km gradient was responsible for the appearance of prehnite, overgrowing epidote and actinolite, and growing inside veins.

7 | DISCUSSION

The CO is a portion of the oceanic lithosphere exhumed at the seafloor of the Alpine Tethys (i.e., the Ligurian-Piedmont ocean) in the Late Jurassic (Manatschal et al., 2022, and references therein). Studies based on mantle compositions through various units of the Alpine Tethys suggest that the CO could belong to the most ocean-ward part of the hyper-extended margin, rather than to a true ocean (Picazo et al., 2016; Rampone & Piccardo, 2000). The opening of the Alpine Tethys has been linked to the development of transform faults and oceanic core complexes along slow-spreading Mid Ocean Ridges (Chalot-Prat & Bourlier, 2005; Festa et al., 2015; Lagabrielle et al., 2015; Lagabrielle & Lemoine, 1997; Manatschal et al., 2011).

In the present tectonic nappe system of Ligurian-Piedmont units, the CO and its underlying Lago Nero unit have been distinguished on the basis of the Alpine mineral assemblages, that in the meta-mafic rocks of the Lago Nero unit are marked by the occurrence of Na-clinopyroxene, phengite, glaucophane, and lawsonite (Koehn & Vuagnat, 1970; Polino et al., 2002). The peak Alpine P–T conditions of the units surrounding the CO have been constrained at 14–18 kbar and 300–400°C for the Lago Nero unit (e.g., Agard et al., 2001; Beyssac et al., 2002) and 4.0–7.5 kbar and 250–300°C for the adjacent continental units of the Houillère Zone (Briançonnais domain; e.g., Lanari et al., 2012). The common hypothesis, reported in Manatschal et al. (2011), to explain the weak Alpine overprint and consequently the excellent preservation of oceanic contacts within the CO, is that it escaped subduction during Alpine convergence and, instead, was thrusted (obducted) onto the proximal European margin and other meta-ophiolite-bearing units.

Our study sheds light on two important aspects concerning the evolution of the CO recording both HT and Alpine (LT-HP) metamorphism: (i) The HT metamorphism and the LT-HP metamorphism are characterized by different micro-structures that developed at different times and (ii) the CO experienced peak metamorphic conditions during the Alpine orogeny at pressures significantly higher than those previously assumed.

7.1 | HT versus Alpine metamorphism

Our petrographic and mineral chemistry data demonstrate that HT metamorphism was recorded only by small bodies of gabbro and other minor plutonic rocks. No evidence of HT micro-structures or mineral assemblages have been found either in the volcanic rocks or in the albitite (i.e., alkali syenite; see Supporting Information S1 for additional details). Therefore, we argue that the HT metamorphism was localized in the small gabbroic bodies bordered by HT shear zones (Nicollet et al., 2022; Tribuzio et al., 2019) and that this HT metamorphic event preceded the volcanic activity. Consequently, the complete absence of a HT metamorphic assemblage in albitites and basalts suggests that they experienced only a LT-HP event. In the Alpine setting in which the CO is set, this LT-HP metamorphism can be linked to subduction processes of inferred Alpine age.

Figure 11 shows the schematic evolution of the gabbro, from its magmatic origin (Figure 11b) to the HT (Figure 11c) and Alpine metamorphism (Figure 11d–g). The HT metamorphism in these rocks was responsible for the widespread blastesis of HT Ca-amphibole (pargasite to hornblende) (Figure 11a–c); further pieces of evidence of HT metamorphism, if any, have been presumably destroyed by Alpine metamorphism.

Our detailed microstructural investigation implies that the low-grade metamorphic minerals pumpellyite, chlorite, actinolite, and prehnite, often interpreted as the product of oceanic seafloor metamorphism (Bertrand et al., 1982; Lewis & Smewing, 1980; Mével et al., 1978; Pusztaszeri, 1966), are instead related to an Alpine low pressure metamorphic event, because they overgrow and/or replace the diagnostic Alpine HP mineral phases (i.e., lawsonite). Although not preserved equally in all the lithologies, the Alpine-related mineral phases occur both in the plutonic and in the volcanic rocks of the CO.

7.2 | Alpine event

In the CO, the Alpine event developed and was better preserved in the lithologies characterized by a low-variant mineral assemblage (i.e., gabbro). In these rocks, the presently observed mineral assemblage is the product of a complex history, consisting of (i) the (partial) preservation of the magmatic mineral assemblage (Figure 11b), (ii) a (presumably Late Jurassic) HT metamorphic event (Figure 11c), and (iii) a multi-stage Alpine metamorphic history consisting of at least four evolutionary steps (Figure 11a,d–g).

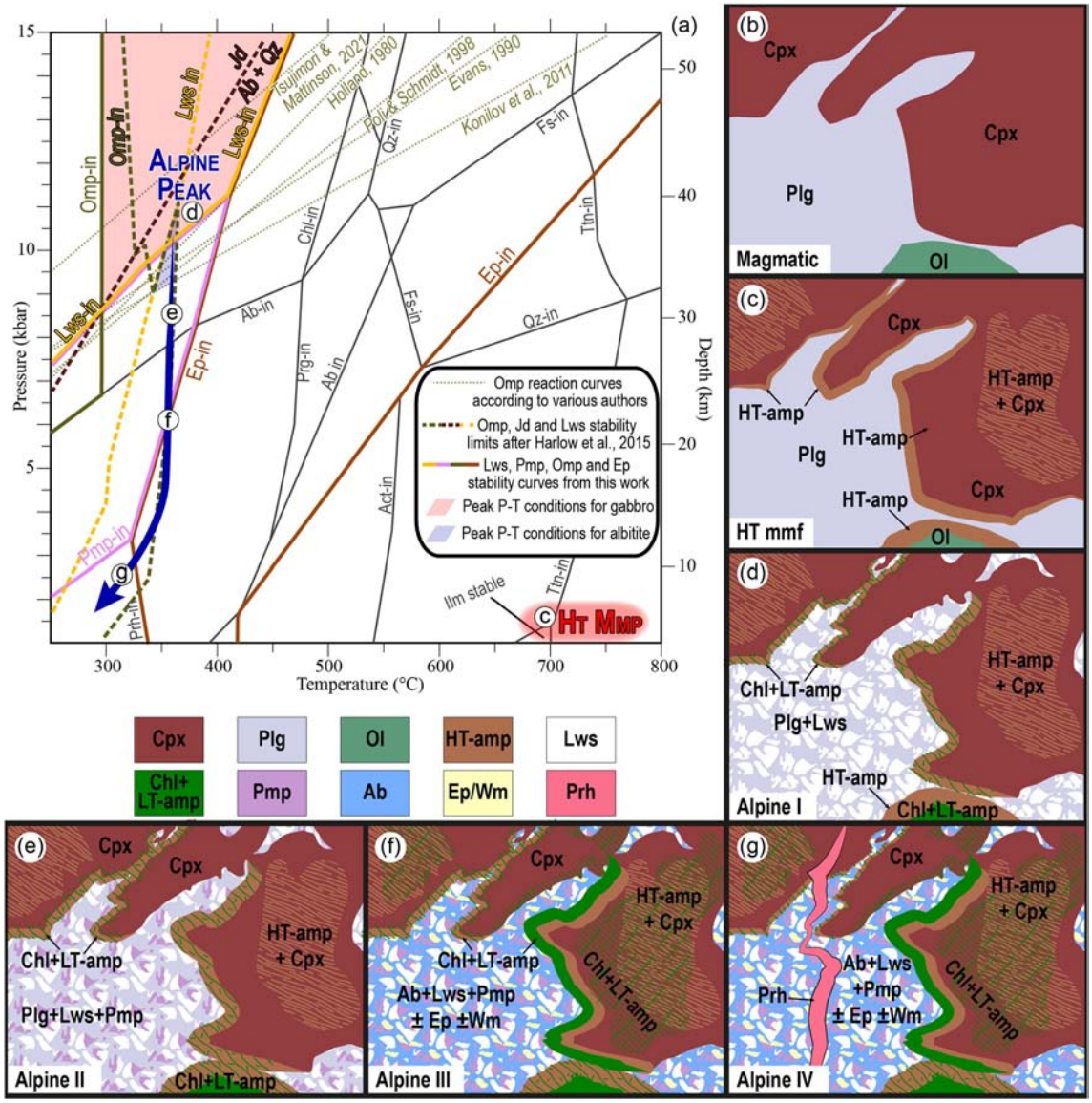

FIGURE 11 Schematic evolution of the gabbro from the Chenaillet Ophiolite. (a) Same isochemical phase diagram reported in Figure 10a,b comprising both the HT-metamorphic event (HT mmp) and the Alpine evolution. The phase-in boundaries modelled for the gabbro sample studied in this work are reported with solid lines, whereas phase-in curves from other authors are reported with dashed lines. Stability curves for lawsonite, pumpellyite, omphacite, and epidote are reported in colours for clearness. The red ellipse shows the constrained P–T conditions for the HT event, based on mineral assemblage. The large, red field in the upper left of the diagram shows the P–T peak conditions inferred for the gabbro sample LG16a based on the results of thermodynamic modelling. Alpine peak P–T conditions are further constrained by the overlap with the P–T peak conditions estimated for the albitite sample (blue field), delimited by the phase-in curves defined for the mafic system according to Harlow et al. (2015) (see text for further details). Letters from (c) to (g) in white circles represent the corresponding stages in the tectono-metamorphic evolution of the rock, reported in the correspondent figures on the right; (b) schematic sketch for the original, magmatic texture of the studied gabbro; (c) HT event in the gabbro, leading to the blastesis of HT-amphiboles over clinopyroxene and olivine; (d) first stage of Alpine metamorphism, characterized by the development of the peak mineral assemblage. Lawsonite grows within the plagioclase sites, whereas Mg-chlorite and LT-amphibole completely replace olivine crystals and grow at the rim of clinopyroxene (+HT-amphibole) crystals; (e) second stage of the Alpine event. Pumpellyite starts to overgrow lawsonite crystals inside plagioclase sites, whereas Mg-chlorite and LT-amphibole continue to grow at rims of clinopyroxene; (f) third stage of the Alpine event. Albite replaces magmatic plagioclase and epidote and white mica starts to grow over lawsonite. In clinopyroxene sites, chlorite and LT-amphibole starts to grow also in fractures; and (g) fourth and last stage of the Alpine event, at the brittle-ductile transition, with blastesis of prehnite in veins cross-cutting the rock. [Colour figure can be viewed at wileyonlinelibrary.com]

The first stage of Alpine metamorphism (Figure 11a,d) is marked by the blastesis of lawsonite in the micro-structural sites of plagioclase in gabbroic rocks and chlorite + actinolite at the expense of HT-amphibole, as well as of magmatic clinopyroxene and olivine crystals. This stage represents the peak P–T conditions reached by the CO and can be constrained to a range of P–T conditions from a minimum of 9 kbar and 300°C to a maximum of 15 kbar and 450°C. These blueschist-facies conditions are further confirmed by the mineral assemblage observed in the albitite of the Col du Gondran, in which the coexistence of albite and omphacite is documented. As reported by Harlow et al. (2015) for the mafic system (Figure 11a), the coexistence of omphacite and albite is limited at P–T conditions lying below and to the left of the omphacite-in curve and below the jadeite-in curve. The absence of lawsonite in the albitite further constrains the P–T conditions on the right side of the lawsonite-in curve, defining a narrow T interval of 340–360°C and $P < 11$ kbar. Overlapping the peak P–T conditions inferred for the albitite with the large stability field of the gabbro assemblage predicted by thermodynamic modelling further constrains peak Alpine metamorphism at 10–11 kbar and 340–360°C (Figure 11d). The predicted peak P–T conditions for the CO plot above the stability curve of omphacite (Figure 11a) as defined in the literature (different reactions: Evans, 1990; Holland, 1980; Konilov et al., 2011; Poli & Schmidt, 1998; Tsujimori & Mattinson, 2021). Hence, based on an average geothermal gradient of 8–10°C/km, we can infer that the CO reached a depth of 35–40 km, which cannot be related to any burial process but must be linked to subduction.

The onset of decompression is witnessed (Figure 11e) by the breakdown of lawsonite, which was mostly overgrown by pumpellyite; this phase presumably occurred at around 9 (±1) kbar and 350 (±25)°C and approximately at 30 km of depth. With the proceeding of decompression, two important reactions occurred (Figure 10a,b,f) which led to the appearance of albite and epidote the (Ab-in and the Ep-in reactions). In the same stage, the clinopyroxene sites experienced the most pervasive retrogression, with the widespread growth of (Mg-)chlorite and actinolite. This event occurred at around 5 ± 1 kbar and 350 ± 25°C, at 20 km of depth. The last effect of Alpine metamorphism is represented by the growth of metamorphic minerals at the brittle-ductile transition, mostly represented by the development of prehnite veins cross-cutting through the rock, at T around 300°C and P lower than 3 kbar (Figure 11g).

8 | CONCLUSIONS AND OPEN QUESTIONS

Thermodynamic modelling performed on a gabbro sample from the CO suggests a minimum of 9 kbar and 300°C and a maximum of 15 kbar and 450°C. Overlapping these P–T conditions with those inferred for the albitite (based on the observed mineral assemblage) allows the Alpine peak metamorphism to be constrained at 10–11 kbar and 340–360°C.

These results point to an Alpine metamorphic history at P–T conditions significantly higher than the (lower) greenschist-facies conditions suggested by a few previous authors (Bertrand et al., 1982; Lewis & Smewing, 1980; Mével et al., 1978; Pusztaszeri, 1966), reaching the LT blueschist-facies conditions for the CO.

This finding opens a series of challenging questions, whose answers require further studies:

i. Evidence of the Alpine HP metamorphism in the CO (marked by the lawsonite and omphacite occurrence) has been found only in the gabbroic and plutonic rocks occurring on top of the serpentinized mantle and below the volcanic cover. Hence, further studies are needed to understand whether these peak P–T conditions can be widened to the whole unit or if the CO actually includes an upper less-metamorphic and a lower more-metamorphic portion.
ii. Alpine metamorphism in the CO seems to have occurred only as static blastesis of HP minerals, without the development of a pervasive schistosity. This requires reconsideration of the relationships between metamorphic evolution and related deformation, possibly also in other external units of the Alpine chain.
iii. The HP Alpine metamorphic evolution of the CO (occurring on top of the nappe stack of Alpine units) opens also a series of implications in terms of models to explain and describe the subduction and exhumation processes of the oceanic units in this sector of the Western Alps.

ACKNOWLEDGEMENTS

An anonymous reviewer and Andy Smye are thanked for their suggestions and helpful feedback, which undoubtedly improved this manuscript. We wish to thank Clare Warren for her excellent editorial job. This work was financially supported by Ministero dell'Università e della Ricerca Scientifica e Tecnologica (M.I.U.R.) in the framework of the PhD project of A.C. Open Access Funding provided by Universita degli Studi di Torino within the CRUI-CARE Agreement.

CONFLICT OF INTEREST STATEMENT

The authors declare that they have no competing interests.

DATA AVAILABILITY STATEMENT

The data that support the findings of this study are available from the corresponding author upon reasonable request.

ORCID

Alberto Corno https://orcid.org/0000-0003-1041-6758
Chiara Groppo https://orcid.org/0000-0002-4174-6613

REFERENCES

Agard, P. (2021). Subduction of oceanic lithosphere in the Alps: Selective and archetypal from (slow-spreading) oceans. *Earth-Science Reviews*, 103517.

Agard, P., Vidal, O., & Goffé, B. (2001). Interlayer and Si content of phengite in HP–LT carpholite-bearing metapelites. *Journal of Metamorphic Geology*, *19*(5), 479–495. https://doi.org/10.1046/j.0263-4929.2001.00322.x

Angiboust, S., & Harlov, D. (2017). Ilmenite breakdown and rutile-titanite stability in metagranitoids: Natural observations and experimental results. *American Mineralogist: Journal of Earth and Planetary Materials*, *102*(8), 1696–1708. https://doi.org/10.2138/am-2017-6064

Arata, J. F., Compagnoni, R., & Sandrone, R. (1982). Caratteri e distribuzione del metamorfismo nei lembi ofiolitici dell'area del Monginevro-Chenaillet (Alpi Cozie). *Rendiconti Della Societa Italiana di Mineralogia e Petrologia*, *38*, 899–899.

Balestro, G., Festa, A., & Dilek, Y. (2019). Structural architecture of the Western Alpine Ophiolites, and the Jurassic seafloor spreading tectonics of the Alpine Tethys. *Journal of the Geological Society*, *176*(5), 913–930. https://doi.org/10.1144/jgs2018-099

Barféty, J. C., Lemoine, M., de Graciansky, P. C., Tricart, P., & Mercier, D. (1995). *Carte géologique de France au 1/50 000, feuille Briançon. Notice explicative*, 180 pp. Bur. Rech. Géol. Min.

Bertrand, J., Courtin, B., & Vuagnat, M. (1982). Elaboration d'un secteur de lithosphère océanique liguro-piémontais d'après les données de l'ophiolite du Montgenèvre (Hautes-Alpes, France et province de Turin). *Ofioliti*, *7*, 155–196.

Bertrand, J., Dietrich, V., Nievergelt, P., & Vuagnat, M. (1987). Comparative major and trace element geochemistry of gabbroic and volcanic rock sequences, Montgenèvre ophiolite, Western Alps. *Schweizerische Mineralogische Und Petrographische Mitteilungen*, *67*, 147–169.

Beyssac, O., Rouzaud, J. N., Goffé, B., Brunet, F., & Chopin, C. (2002). Graphitization in a high-pressure, low-temperature metamorphic gradient: A Raman microspectroscopy and HRTEM study. *Contributions to Mineralogy and Petrology*, *143*, 19–31. https://doi.org/10.1007/s00410-001-0324-7

Bocchio, R., Benciolini, L., Martin, S., & Tartarotti, P. (2000). Geochemistry of eclogitised Fe-Ti-gabbros from various lithological settings (Aosta Valley ophiolites, Italian western Alps). Protolith composition and eclogitic paragenesis. *Periodico di Mineralogia*, *69*(3), 217–237.

Bucher, K., Fazis, Y., De Capitani, C., & Grapes, R. (2005). Blueschists, eclogites, and decompression assemblages of the Zermatt-Saas ophiolite: High-pressure metamorphism of subducted Tethys lithosphere. *American Mineralogist*, *90*(5–6), 821–835. https://doi.org/10.2138/am.2005.1718

Bucher, K., & Grapes, R. (2009). The eclogite-facies Allalin gabbro of the Zermatt–Saas ophiolite, Western Alps: A record of subduction zone hydration. *Journal of Petrology*, *50*(8), 1405–1442. https://doi.org/10.1093/petrology/egp035

Buffon, G. (1786) *Histoire naturelle des minéraux*. Imprimerie royale. T. iv., 395 p. Paris.

Burroni, A., Levi, N., Marroni, M., & Pandolfi, L. (2003). Lithostratigraphy and structure of the Lago Nero unit (Chenaillet massif, western Alps): Comparison with internal liguride units of northern Apennines. *Ofioliti*, *28*(1), 1–11.

Caby, R. (1995). Plastic deformation of gabbros in a slow-spreading Mesozoic Ridge: Example of the Montgenèvre Ophiolite. In R. L. M. Vissers & A. Nicolas (Eds.), *Mantle and lower crust exposed in oceanic ridges and in ophiolites* (pp. 123–145). Kluwer Academic Publishers. https://doi.org/10.1007/978-94-015-8585-9_5

Chalot-Prat, F. (2005). An undeformed ophiolite in the Alps: Field and geochemical evidence for a link between volcanism and shallow plate tectonic processes. In: Foulger, G.R., Natland, J.H., Presnall, D.C., Anderson, D.L. (Eds.), plates, plumes and paradigms. *Geological Society of America Special Papers*, *388*, 751–780. https://doi.org/10.1130/0-8137-2388-4.751

Chalot-Prat, F., & Bourlier, E. C. Y. (2005). *L'ophiolite du Chenaillet (Montgenèvre, Alpes franco-italiennes), témoin d'un segment de ride volcanique axiale d'un océan à croissance lente*. Géol.

Connolly, J. A. D. (1990). Multivariable phase diagrams: An algorithm based on generalized thermodynamics. *American Journal of Science*, *290*, 666–718. https://doi.org/10.2475/ajs.290.6.666

Connolly, J. A. D. (2005). Computation of phase equilibria by linear programming: A tool for geodynamic modeling and its application to subduction zone decarbonation. *Earth and Planetary Science Letters*, *236*(1–2), 524–541. https://doi.org/10.1016/j.epsl.2005.04.033

Connolly, J. A. D. (2009). The geodynamic equation of state: What and how. *Geochemistry, Geophysics, Geosystems*, *10*(10), 1, n/a–19. https://doi.org/10.1029/2009GC002540

Costa, S., & Caby, R. (2001). Evolution of the Ligurian Tethys in the Western Alps: Sm/Nd and U/Pb geochronology and rare-earth element geochemistry of the Montgenèvre ophiolite (France). *Chemical Geology*, *175*, 449–466. https://doi.org/10.1016/S0009-2541(00)00334-X

Deer, W. A., Howie, R. A., & Zussman, J. (1997). *Rock-forming minerals*. Geol. Soc. Lond, U.K. Longmane. 528 p.

Delesse. (1848). Sur la variolite de la Durance. *Bull. Soc. Géol. France*, *2*(VII), 427–431.

Evans, B. W. (1990). Phase relations of epidote-blueschists. *Lithos*, *25*, 3–23. https://doi.org/10.1016/0024-4937(90)90003-J

Festa, A., Balestro, G., Dilek, Y., & Tartarotti, P. (2015). A Jurassic oceanic core complex in the high-pressure Monviso ophiolite (western Alps, NW Italy). *Lithosphere*, *7*(6), 646–652. https://doi.org/10.1130/L458.1

Fuhrman, M. L., & Lindsley, D. H. (1988). Ternary-feldspar modeling and thermometry. *American Mineralogist*, *73*(3–4), 201–215.

Green, E., Holland, T., & Powell, R. (2007). An order-disorder model for omphacitic pyroxenes in the system jadeite-

diopside-hedenbergite-acmite, with applications to eclogitic rocks. *American Mineralogist*, *92*(7), 1181–1189. https://doi.org/10.2138/am.2007.2401

Green, E. C. R., White, R. W., Diener, J. F. A., Powell, R., Holland, T. J. B., & Palin, R. M. (2016). Activity–composition relations for the calculation of partial melting equilibria in metabasic rocks. *Journal of Metamorphic Geology*, *34*(9), 845–869. https://doi.org/10.1111/jmg.12211

Harlow, G. E., Tsujimori, T., & Sorensen, S. S. (2015). Jadeitites and plate tectonics. *Annual Review of Earth and Planetary Sciences*, *43*, 105–138. https://doi.org/10.1146/annurev-earth-060614-105215

Hawthorne, F. C., Oberti, R., Harlow, G. E., Maresch, W. V., Martin, R. F., Schumacher, J. C., & Welch, M. D. (2012). Nomenclature of the amphibole supergroup. *American Mineralogist*, *97*(11–12), 2031–2048. https://doi.org/10.2138/am.2012.4276

Holland, T. J. B. (1980). The reaction albite = jadeite + quartz determined experimentally in the range 600-1200°C. *American Mineralogist*, *65*, 129–134.

Holland, T. J. B., & Powell, R. (1998). An internally consistent thermodynamic dataset for phases of petrological interest. *Journal of Metamorphic Geology*, *16*, 309–343. https://doi.org/10.1111/j.1525-1314.1998.00140.x

Holland, T. J. B., & Powell, R. (2011). An improved and extended internally consistent thermodynamic dataset for phases of petrological interest, involving a new equation of state for solids. *Journal of Metamorphic Geology*, *29*, 333–383. https://doi.org/10.1111/j.1525-1314.2010.00923.x

Koehn, P., & Vuagnat, M. (1970). Sur la présence du faciès "schistes à glaucophane" dans les roches du Mt. Cruzeau (Province de Turin, Italie). *CR Des Séances, SPHN, Genevé*, *5*, 59–64.

Konilov, A. N., Shchipansky, A. A., Mints, M. V., Dokukina, K. A., Kaulina, T. V., Bayanova, T. B., Natapov, L. M., Belousova, E. A., Griffin, W. L., & O'Reilly, S. Y. (2011). The Salma eclogites of the Belomorian Province, Russia: HP/UHP metamorphism through the subduction of Mesoarchean oceanic crust. In *Ultrahigh-pressure metamorphism* (pp. 623–670). Elsevier.

Lafay, R., Baumgartner, L. P., Stephane, S., Suzanne, P., German, M. H., & Torsten, V. (2017). Petrologic and stable isotopic studies of a fossil hydrothermal system in ultramafic environment (Chenaillet Ophicalcites, Western Alps, France): Processes of carbonate cementation. *Lithos*, *294*, 319–338. https://doi.org/10.1016/j.lithos.2017.10.006

Lagabrielle, Y., Brovarone, A. V., & Ildefonse, B. (2015). Fossil oceanic core complexes recognized in the blueschist metaophiolites of Western Alps and Corsica. *Earth-Science Reviews*, *141*, 1–26. https://doi.org/10.1016/j.earscirev.2014.11.004

Lagabrielle, Y., & Lemoine, M. (1997). Alpine, Corsican and Apennine ophiolites: The slow-spreading ridge model. *Comptes Rendus de l'Académie Des Sciences - Series IIA - Earth and Planetary Science*, *325*(12), 909–920. https://doi.org/10.1016/S1251-8050(97)82369-5

Lagabrielle, Y., & Polino, R. (1988). Un schéma structural du domaine des Schistes lustrés ophiolitifères au nord-ouest du massif du Mont Viso (Alpes Sud-Occidentales) et ses implications (a structural map of the ophiolite-bearing 'Schistes lustrés' northwest of the Monte Viso massif (SW Alps) and its implications). *Comptes Rendus de l'Académie Des Sciences [Paris], Série*, *2*(306), 921–928.

Lanari, P., Guillot, S., Schwartz, S., Vidal, O., Tricart, P., Riel, N., & Beyssac, O. (2012). Diachronous evolution of the alpine continental subduction wedge: Evidence from P-T estimates in the Briançonnais Zone houillère (France–Western Alps). *Journal of Geodynamics*, *56*, 39–54. https://doi.org/10.1016/j.jog.2011.09.006

Lanari, P., Vho, A., Bovay, T., Airaghi, L., & Centrella, S. (2019). Quantitative compositional mapping of mineral phases by electron probe micro-analyser. *Geological Society of London, Special Publication*, *478*, 39–63. https://doi.org/10.1144/SP478.4

Leake, B. E., Woolley, A. R., Arps, C., Birch, W. D., Gilbert, M. C., Grice, J. D., Hawthorne, F. C., Kato, A., Kisch, H. J., Krivovichev, V. G., Linthout, K., Laird, J., Mandarino, J., Maresch, W. V., Nickel, E. H., Rock, N. M. S., Schumacher, J. C., Smith, D. C., Stephenson, N. C. N., ... Youzhi, G. (1997). Nomenclature of amphiboles. *American Mineralogist*, *82*, 1019–1037.

Lemoine, M. (1980). Serpentinites, gabbros and ophicalcites in the Piemont-Ligurian domain of the Western Alps: Possible indicators of oceanic fracture zones and of associated serpentinite protrusions in the Jurassic-Cretaceous Tethys. *Archives des Sciences*, *33*(2-3), 103–115.

Lewis, A. D., & Smewing, J. D. (1980). The Montgenèvre ophiolite (Hautes-Alpes, France): Metamorphism and trace element geochemistry of the volcanic sequence. *Chemical Geology*, *28*, 291–306. https://doi.org/10.1016/0009-2541(80)90050-9

Li, X. H., Faure, M., Lin, W., & Manatschal, G. (2013). New isotopic constraints on age and magma genesis of an embryonic oceanic crust: The Chenaillet Ophiolite in the Western Alps. *Lithos*, *160-161*, 283–291. https://doi.org/10.1016/j.lithos.2012.12.016

Manatschal, G., Chenin, P., Haupert, I., Masini, E., Frasca, G., & Decarlis, A. (2022). The importance of rift inheritance in understanding the early collisional evolution of the Western Alps. *Geosciences*, *12*(12), 434. https://doi.org/10.3390/geosciences12120434

Manatschal, G., Sauter, D., Karpoff, A. M., Masini, E., Mohn, G., & Lagabrielle, Y. (2011). The Chenaillet Ophiolite in the French/Italian Alps: An ancient analogue for an oceanic core complex? *Lithos*, *124*, 169–184. https://doi.org/10.1016/j.lithos.2010.10.017

Martin, R. (1984). Patterns of albitization in the Montgenèvre ophiolite, Western Alps. *Bulletin de Mineralogie*, *107*(3), 345–356. https://doi.org/10.3406/bulmi.1984.7765

Mevel, C. (1975). *Les "pillow-lavas" spilitiques des massifs ophiolitiques du Chenaillet et des Gets (Alpes françaises). Structures et minéraux magmatiques reliques, étude chimique et zonations Comparaison avec les "pillow-lavas" métamorphisés du Queyras et de Hte Ubaye* (Doctoral dissertation. Université Pierre et Marie Curie-Paris VI.

Mével, C., Caby, R., & Kienast, J.-R. (1978). Amphibolite-facies conditions in the oceanic crust: Example of amphibolized flaser-gabbro and amphibolites from the Chenaillet ophiolite massif (Hautes Alpes, France). *Earth and Planetary Science Letters*, *39*, 98–108. https://doi.org/10.1016/0012-821X(78)90146-2

Mevel, C., & Velde, D. (1976). Clinopyroxenes in Mesozoic pillow lavas from the French Alps: Influence of cooling rate on compositional trends. *Earth and Planetary Science Letters*, *32*(2), 158–164. https://doi.org/10.1016/0012-821X(76)90054-6

Michel-Lévy, A. (1877). *Structure et composition minéralogique de la variolite de la Durance* (pp. 264–266). C.R. LXXXIV, Soc. Géol.

Montanini, A., Tribuzio, R., & Vernia, L. (2008). Petrogenesis of basalts and gabbros from an ancient continent–ocean transition (External Liguride ophiolites, Northern Italy). *Lithos*, *101* (3-4), 453–479.

Morimoto, N. (1988). Nomenclature of pyroxenes. *Schweizerische Mineralogische Und Petrographische Mitteilungen*, *68*, 95–111.

Nicollet, C., Paquette, J. L., Bruand, E., Bosse, V., & Pereira, I. (2022). Crystallisation and fast cooling of the (meta)gabbro from the Chenaillet ophiolite (Western Alps): In-situ U–Pb dating of zircon, titanite, monazite and xenotime in textural context. *Lithos*, *414–415*, 106620. https://doi.org/10.1016/j.lithos.2022.106620

Picazo, S., Müntener, O., Manatschal, G., Bauville, A., Karner, G., & Johnson, C. (2016). Mapping the nature of mantle domains in Western and Central Europe based on clinopyroxene and spinel chemistry: Evidence for mantle modification during an extensional cycle. *Lithos*, *266*, 233–263. https://doi.org/10.1016/j.lithos.2016.08.029

Poli, S., & Schmidt, M. W. (1998). The high-pressure stability of zoisite and phase relationships of zoisite-bearing assemblages. *Contributions to Mineralogy and Petrology*, *130*(2), 162–175. https://doi.org/10.1007/s004100050357

Polino, R., Borghi, A., Carraro, F., Dela Pierre, F., Fioraso, G. & Giardino, M. (2002). *Note illustrative della carta geologica d'Italia alla scala 1: 50.000–foglio 132–152-153 "Bardonecchia"*. Litografia Geda, Nichelino.

Polino, R., & Lemoine, M. (1984). Détritisme mixte d'origine continentale et océanique dans les sédiments jurassico-crétacés supra-ophiolitiques de la Téthys ligure: La série du Lago Nero (Alpes Occidentales franco-italiennes). Comptes-rendus des séances de l'Académie des sciences. *Série 2, Mécanique-Physique, Chimie, Sciences de l'univers, Sciences de la Terre*, *298*(8), 359–364.

Polino, R., Monticelli, F., & Vaccaro, D. (1983). L'unità piemontese Chaberton-Grand Hoche (Val Susa-Alpi Occidentali): Evoluzione litostratigrafica, assetto strutturale e rapporti con i complessii circostanti. *Memorie Della Societa Geologica Italiana*, *26*(2), 489–498.

Pusztaszeri, L. (1966). *Etude pétrographique du massif du Chenaillet (Hautes-Alpes, France)*. University of Genève. 468 p.

Rampone, E., & Piccardo, G. B. (2000). The ophiolite–oceanic lithosphere analogue: New insights from the Northern Apennines (Italy). In Y. Dilek, E. M. Moores, D. Elthon, & A. Nicolas (Eds.), *Ophiolites and oceanic crust: New insights from field studies and the oceanic drilling program* (Vol. 349, pp. 21–34). Geological Society of America Special Papers. https://doi.org/10.1130/0-8137-2349-3.21

Shi, R., Yang, J., Xu, Z., & Qi, X. (2008). The Bangong Lake ophiolite (NW Tibet) and its bearing on the tectonic evolution of the Bangong–Nujiang suture zone. *Journal of Asian Earth Sciences*, *32*(5-6), 438–457.

Tribuzio, R., Manatschal, G., Renna, M. R., Ottolini, L., & Zanetti, A. (2019). Tectonomagmatic interplay and related metasomatism in gabbros from the Chenaillet ophiolite (Western Alps). *Journal of Petrology*, *60*, 2483–2508. https://doi.org/10.1093/petrology/egaa015

Tsujimori, T., & Mattinson, C. (2021). Eclogites in different tectonic settings. In S. Elias & D. Alderton (Eds.), *Encyclopedia of geology* (2nd ed., pp. 561–568). Academic Press. https://doi.org/10.1016/B978-0-08-102908-4.00104-1

Vuagnat, M. (1946). Sur quelques diabases suisses. Contribution à l'étude des spillites et des pillows lavas. *BSMP*, *26*, 116–128.

Vuagnat, M. (1966). Les coussins éclatés du Lago Nero (Massif du Montgenèvre, Prov. de Turin) et le problème des brèches ophiolitiques (note préliminaire). *Compte Rendu Des séances de la Société de Physique et d'histoire Naturelle de Genève*, *3*, 163–167.

Vuagnat, M. (1975). Pillow lava flows: Isolated sacks or connected tubes? *Bulletin Volcanologique*, *39*(4), 581–589. https://doi.org/10.1007/BF02596978

Vuagnat, M., & Pusztaszeri, L. (1965). Sur la presence de hyaloclastites dans le massif du Mont-Genèvre (H.-A.). *Archives Des Sciences Genève*, *18*(1), 120–123.

White, R. W., Powell, R. O. G. E. R., Holland, T. J. B., Johnson, T. E., & Green, E. C. R. (2014). New mineral activity–composition relations for thermodynamic calculations in metapelitic systems. *Journal of Metamorphic Geology*, *32*(3), 261–286. https://doi.org/10.1111/jmg.12071

Whitney, D. L., & Evans, B. W. (2010). Abbreviations for names of rock-forming minerals. *American Mineralogist*, *95*(1), 185–187. https://doi.org/10.2138/am.2010.3371

SUPPORTING INFORMATION

Additional supporting information can be found online in the Supporting Information section at the end of this article.

Appendix S1. Description of the main petrographic, textural and mineral chemical features of pillow basalt and dolerite dikes and sills.

Figure S1. a-b) P-M(H_2O) (mol%) isochemical phase diagrams calculated at T = 300°C (a) and T = 350°C (b) for sample LG16a. The observed peak mineral assemblage (red fields) is stable only at H_2O-saturated conditions (blue dotted area) or at very slight H_2O-undersaturated conditions; c-d) P-X (Fe_2O_3) isochemical phase diagrams calculated at T = 300°C (c) and T = 350°C (d) for sample LG16a. X (Fe_2O_3) is defined as $Fe_2O_3/(FeO + Fe_2O_3)$ [i.e. X (Fe_2O_3) = 0 means that all Fe is bivalent]. The two diagrams show that, increasing the oxidation state of the system, the observed peak mineral assemblage (red field) is stable at progressively higher P and it is no more stable for X (Fe_2O_3).

Figure S2. Modelled volume% of each mineral phase. The colour coded scalebar is proportional for each mineral, from its minimum to its maximum amount, and it is not fixed. Corresponding minimum-maximum values for each mineral phase are reported above each diagram. This figure helps to better constrain the exhumation path, supporting of pie diagrams of Figure 10c. Please refer to Figure 10a,b for the labels of each field. Numeric key: 1 = Cpx + Chl + Omp + Amp1 + Lws + Ttn; 2 = Cpx + Amp1 + Chl + Lws + Ttn; 3 = Cpx + Amp1

+ Chl + Zo + Ttn; 4 = Cpx + Amp1 + Amp2 + Zo + Ttn; 5 = Cpx + Amp2 + Plg + Zo + Ttn + Qz; 6 = Cpx + Amp2 + Zo + Ttn + Qz; 7 = Cpx + Amp1 + Amp2 + Ep + Ttn + Qz; 8 = Cpx + Amp2 + Plg + Ttn + Qz; 9 = Cpx + Amp1 + Amp2 + Ab+Ep + Ttn + Qz; 10 = Cpx + Amp1 + Amp2 + Plg + Zo + Ttn; 11 = Cpx + Amp1 + Amp2 + Ab+Ttn + Zo; 12 = Cpx + Amp1 + Chl + Ttn + Ab+Ep; 13 = Cpx + Pmp + Amp1 + Ttn + Qz; 14 = Cpx + Omp + Amp1 + Pmp + Ttn + Qz; 15 = Cpx + Amp1 + Pmp + Chl + Ttn + Ab; 16 = Cpx + Amp1 + Chl + Czo + Ttn + Ab; 17 = Cpx + Amp1 + Chl + Prh + Ttn + Ab; 18 = Cpx + Amp1 + Amp2 + Plg + Ttn; 19 = Cpx + Amp2 + Plg + Ttn; 20 = Cpx + Amp2 + Plg + Ilm.

Table S1. Clinopyroxene representative analyses.

Table S2. Lawsonite representative analyses.

Table S3. Amphibole representative analyses.

Table S4. Pumpellyite representative analyses.

Table S5. Chlorite and white mica representative analyses.

Table S6. Plagioclase and epidote representative analyses.

How to cite this article: Corno, A., Groppo, C., Borghi, A., Mosca, P., & Gattiglio, M. (2023). To be or not to be Alpine: New petrological constraints on the metamorphism of the Chenaillet Ophiolite (Western Alps). *Journal of Metamorphic Geology*, 1–21. https://doi.org/10.1111/jmg.12716